MEAN FLOW AND TURBULENCE MEASUREMENTS IN THE WAKE OF A SLENDER PROPELLER-DRIVEN BODY INCLUDING EFFECTS OF PITCH ANGLE

by

Edward Bruce Daffan

Thesis submitted to the Graduate Faculty of the
Virginia Polytechnic Institute and State University
in partial fulfillment of the requirements for the degree of
MASTER OF SCIENCE
in
Aerospace Engineering

APPROVED:

J. A. Schetz, Chairman

A. K. Jakubowski

E. M. Cliff

June, 1976

Blacksburg, Virginia

ACKNOWLEDGEMENTS

I would like to thank Dr. Schetz and my other professors for their technical advice and guidance throughout this project. My special thanks to my typist, Miss Vicki Price, for her very professional typing and to Rick Robinson and Urs Keller for preparation of many of the detailed figures. Most of all, I thank my wife, Cindy, for her patience and understanding while preparing this report.

TABLE OF CONTENTS

NOMENCLATURE

ALPHA	geometric pitch angle of model
$b_{1/2}$	width from wake center to wake edge
C_D	drag coefficient
D	maximum diameter of model
E	D.C. voltage
e	RMS voltage
FP	flow pitch angle
FY	flow yaw angle
K_β	probe coefficient for flow yaw
K_α	probe coefficient for flow pitch
K_i	hole coefficient
P_B	barometric pressure
P_i	probe hole pressure
P_{st}	static pressure
$P_{st\infty}$	freestream static pressure
P_o	total pressure
q	dynamic pressure
Q	dynamic pressure
Q_E	dynamic pressure at edge of wake
R	model maximum radius
RPM	revolutions per minute
R_e	Reynolds number
Re_D	Reynolds number based on model diameter

U_E	axial velocity at edge of wake
U_z	axial velocity
$\overline{u'}$	mean axial velocity fluctuations
$\overline{u'v'}$	radial shear stress
V_{Total}	total velocity
$\overline{V'}$	total velocity fluctuations
$\overline{v'}$	mean radial velocity fluctuations
x, y, z	coordinate directions
ρ	density
α_e	effective model pitch angle
$\overline{w'^2}$	mean tangential velocity fluctuations

LIST OF FIGURES

Page

Page

I. INTRODUCTION

The study of the turbulent wake produced by propeller-driven bodies and its application in the detection of submersibles has become of increasing interest in recent years. The wake produced by a propeller-driven submersible can extend many body diameters downstream and can therefore effectively increase the target of detection. Most of the past work on axisymmetric wake flows has dealt with general shapes such as circular disks, ellipsoids, spheroids, and some slender bodies. The majority of these studies however have dealt with unpropelled configurations.

The work on propelled bodies has been primarily restricted to jets injected from circular disks such as the works by Ridjanovic[1] and Naudascher[2]. Only in the last two years has the wake of propeller-driven bodies been considered. Gran[3] in 1974 studied the wake of a propeller-driven Rankine Ovoid at Reynolds numbers based on diameter of $\simeq 6 \times 10^4$. More extensive work on propeller-driven slender bodies was published in 1974 by Swanson[4], et. al., and Chieng[5], et. al., at Re_D of $\simeq 6.18 \times 10^5$. From these studies it was found that dramatic changes occur in the wakes of non-propelled slender bodies and self-propelled bodies of the same configuration. The following table gives a survey of past wake studies on axisymmetric bodies.

In this report two previously unstudied effects on the turbulent wakes of propeller-driven bodies are examined. The first is the addition of an appendage to an axisymmetric body and how it effects

TABLE 1

Summary of Subsonic, Axisymmetric Turbulent Wake Experiments

Author	Year	Ref. No.	Momentumless	Mean Flow	Turbulent Properties	Configuration
Hall and Hislop	1938	11		x		1 x 2 Cylinder
Cooper and Lutzky	1955	12		x	x	Thin Disks
Ilizarova and Pochkina	1962	13		x		6.67 x 1 Body of Revolution
Ridjanovic	1963	1	x	x	x	Circular Disk
Carmody	1964	14		x	x	Circular Disk
Wang	1965	15	x	x	x	Circular Disk
Naudascher	1965	2	x	x	x	Circular Disk
Ginevskii, Pochkina, and Ukhanova	1966	16	x	x	x	Circular Disk
Buchinskaya and Pochkina	1966	17		x		6 x 1 Ellipsoid
Chevray	1968	18		x	x	6 x 1 Spheroid

TABLE 1 (Continued)

Summary of Subsonic, Axisymmetric Turbulent Wake Experiments

Author	Year	Ref. No.	Momentumless	Mean Flow	Turbulent Properties	Configuration
Bukreev, Kostomakha, and Lytkin	1972	19		x	x	Slender Body (8:1 Prolongation)
Hokenson and Schetz	1973	20		x	x	Sphere
Bukreev, Kostomakha, and Lytkin	1974	21		x	x	Sphere and Slender Body
Gran	1974	3	x	x	x	Rankine Ovoid
Swanson and Chieng	1974	4,5	x	x	x	Slender Bodies
Daffan and Schetz	1976	Present	x	x	x	Slender Body

the mean flow and turbulence quantities in the wake. The second is the effect of pitch angle on the wake properties.

For this work a less "classical" and more realistic body shape was chosen. A model fineness ratio of 12:1 was chosen because of its similarity to most modern submarines, and the appendage used was scaled to simulate a submarine sail. To study the effect of pitch angle on the wake properties the tests were conducted at model pitch angles of 0° and -2°. The -2° pitch angle was chosen because submarines often operate at a positive buoyancy level as a safety precaution and therefore must cruise at a small negative pitch angle to remain in equilibrium. Also, other self-propelled bodies seldom operate completely level due to changes in velocity and maneuvering.

The testing was conducted in the VPI six-foot, subsonic wind tunnel at $Re_D \simeq 4.4 \times 10^5$. The wind tunnel has proven in the past to be the best facility for detailed pressure and turbulence measurements because of its low free-stream turbulence level and its uniform pressure field. Measurements of total pressure, static pressure, flow angularity, axial turbulence, radial turbulence, and radial shear stress were made at discrete points across the wake at three downstream stations; 2, 10, and 40 model diameters. These measurements then yielded the velocity components; axial turbulence intensity, radial turbulence intensity, and radial shear stress through the wake. The measurements were taken using a yawhead pressure probe, a straight hot-wire sensor, and a cross-wire sensor.

The results are presented in both tabulated and graphical form, and comparisons with previous work on propeller-driven bodies are given whenever applicable.

II. EXPERIMENTAL MODELS AND METHODS

Facility

All tests were conducted in the VPI&SU 6' x 6' subsonic stability tunnel at a dynamic pressure of 5.0 inches of water (approximately 157 ft./sec.) yielding a Re_D based on diameter 4.4 x 10^5. The facility is a continuous closed jet single return wind tunnel. Its test section is 28 ft. long allowing wake measurements at 40 model diameters. The air stream has a low turbulence factor of 1.08. To control the tunnel velocity a Barocel Electric Manometer is used to read dynamic pressure from a pitot-static tube mounted on the test section wall out of the wake of the model. Free-stream temperature is monitored by a temperature probe on the test section wall and recorded on a Digitemp temperature guage. Static free-stream pressure is measured by a Validyne digital barometer Model DB99.

Model

The model considered in this investigation has an overall length of 72 inches and a maximum diameter of 6 inches, giving a fineness ratio of 12:1. The model was strut mounted from the ceiling of the wind tunnel just forward of the test section (Fig. 1). The forebody is parabolic and machined from laminated layers of plexiglas. The centerbody is an aluminum cylindrical tube with a simulated sail, and the tail body is also plexiglas machined into an ogival shape. For the overall dimensions of the body, see Fig. 2.

The model used a 2.75 h.p. DC motor to direct drive the single propeller shaft which extended through the center of the tail section (Fig. 3). A 6 inch diameter, 3 bladed model airplane propeller, was used to provide enough thrust to obtain a self-propelled configuration. The propeller was heated at its root and twisted to a higher pitch to operate more efficiently at the high air speeds used. The effective pitch of the propeller as modified was 2.46 as determined by Swanson in Reference 4.

To avoid overheating for long duration experiments, the motor was encased by copper tubing to allow for water cooling. It should be noted that water cooling was only used for wake measurements and was not used in obtaining the force measurements for the self-propelled status.

To measure propeller rpm, a magnetic pickup was attached near the propeller shaft and the signal was monitored on a Beckman Counter, Model 2D-3. To power the DC motor, a Sorenson 150 volt, 15 amp power supply was used (Fig. 4).

Pressure Probes

The mean flow measurements were made using a three-dimensional Yawhead probe constructed by United Sensor. The probe was used in the wake region when substantial flow angularity occurred (Fig. 5). In the far wake, the flow angularity was sufficiently small to use a standard straight pitot-static tube (Fig. 6).

The output from the pressure probes was measured on a Barocel Electronic Manometer and displayed on a Doric Digital Voltmeter. Graphical displays were provided by a HP 7100B Strip Chart Recorder and a Model 20-3 X-Y Recorder. To read all five pressure ports from the yawhead probe on the electronic manometer, a Scanivalve Model W0601/IP-RT fluid switch wafer with solenoid drive was used.

Hot Wire Instrumentation

The axial turbulence data was obtained using a straight hot wire (TSI Model 1210). This sensor uses a platinum plated tungsten wire .00015 inches in diameter. The probe was operated at an overheat ratio of 1.8 using a constant temperature anemometer module (TSI Model 1050) and a Power Supply and Monitor (TSI Model 1051-6). Readings were taken from a DISA 55D35 RMS Meter. The radial turbulence and radial shear stress were measured using a cross-wire (TSI Model 1241T1.5) similar in construction to the straight wire. A Model 1015C correlator and TSI Model 1076 Voltmeter were also used.

Traverse Mount

Both pressure and hot wire probes were moved through the wake using the traverse shown in Fig. 7. This mount had a vertical movement of 4 ft. and a horizontal range of 11.0 in. It was therefore necessary in the far wake studies to move the mount to obtain a wider horizontal range. Both vertical and horizontal movement was accomplished with

variable speed motors which were controlled outside the test section. The probe position was monitored using a series of potentiometers. For the hot wire measurements it was necessary to rotate the probes. This was done using a small remotely controlled DC motor.

Obtaining Self-Propelled Status

To determine a self-propelled configuration a strain gage balance was internally mounted in the model (Fig. 8). With the model mounted in the tunnel, potentiometers were used to zero the output from the balance due to the weight of the model.

The free-stream velocity was increased to 5.0 inches of water while the axial force was monitored. The propeller rpm was then increased until the axial force reading was zero. This was done for several angles of attack between -6° and +6°. At each angle the propeller RPM needed to zero the axial force was recorded. It was determined that for angles between -2° and +2° a propeller RPM of 14,890 was needed to reach a self-propelled status. This corresponded to an advance ratio of 1.25 and a propeller efficiency of .75 from Ref. 4.

Mean Flow

The mean flow velocities as well as flow angularity were determined using a five-port yawhead probe. This probe was first calibrated over a range of flow pitch and flow yaw angles between -30° and +30° (Figs. 9 and 10).

It was decided that an adequate description of the wake could be achieved with three traverses. These were a vertical traverse through the vertical plane of symmetry, a horizontal cut across the center of the propeller hub, and a horizontal cut across the sail. These cuts are seen in the following schematic.

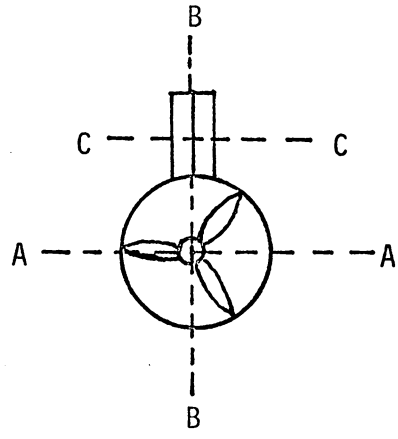

AA - Horizontal cut

BB - Vertical cut

CC - Cut across sail

These three traverses were made at downstream stations of Z/D = 2, 10, and 40 with the model at $\alpha_e = 0°$ and $\alpha_e = -2°$. Measurements were taken at 0.5 inch intervals across the wake. To obtain the mean velocity components from the pressure measurements the following relation for total pressure was used:

$$P_o = P_s + \frac{1}{2}\rho V^2 + \frac{1}{2}\rho \overline{V}'^2$$

where V is the mean total velocity and $\overline{V}'$ is the sum of the mean fluctuations. Since $V^2 >> \overline{V}'^2$ the $\frac{1}{2}\rho \overline{V}'^2$ was neglected. The yaw-head probe gave direct readings of $P_1 - P_{st\infty}$, where P_1 is the mean total pressure and $P_{st\infty}$ is the free stream static pressure.

Therefore since

$$P_1 = P_{st} + \frac{1}{2}\rho V^2$$

the mean total velocity can be calculated from

$$V_{total} = \sqrt{\frac{2[(P_1 - P_{st\infty}) - (P_{st} - P_{st\infty})]}{\rho}}$$

then the mean axial velocity can be obtained by

$$U_z = V\cos(FP)\cos(FY)$$

where FP is the flow pitch angle and FY is the flow yaw angle. Similarly the other velocity components are given by

$$U_x = V\cos(FP)\sin(FY)$$

$$U_y = V\sin(FP)$$

To obtain the local static pressure from the yawhead probe a method described by Winternitz (Ref. 6) was used. Since this method is only good for substantial flow angularity in one direction, calibration curves were obtained for both flow pitch and yaw. The flow yaw angle FY is found from the calibration probe constant

$$K_\beta = \frac{P_3 - P_2}{P_1 - P_4}$$

for each station. Defining the hole constant as

$$K_i(\beta) = \frac{P_i - P_{st}}{q}$$

where P_i is the hole pressure and q is the dynamic pressure. Winternitz showed that

$$q = \frac{(P_1 - P_{st\infty}) - (P_2 - P_{st\infty})}{K_1 - K_2}$$

or

$$(P_{st} - P_{st\infty}) = (P_2 - P_{st\infty}) - qK_2.$$

Therefore

$$(P_{st} - P_{st\infty}) = \frac{K_1(P_2 - P_{st\infty}) - K_2(P_1 - P_{st\infty})}{K_1 - K_2}$$

Similarly for the pitched case where the yaw angles are small

$$K_\alpha = \frac{P_4 - P_5}{P_1 - P_2}$$

and,

$$(P_{st} - P_{st\infty}) = \frac{K_1(P_5 - P_{st\infty}) - K_5(P_1 - P_{st\infty})}{K_1 - K_5}.$$

From these relations the local static pressure could be determined when there was substantial pitch angles with small yaw angles or for large yaw angles with small variations in pitch.

Turbulence Measurements

The axial and radial turbulence intensity and radial shear stress was measured at the same points as the mean flow measurements using both a straight hot wire and a cross-wire. The constant temperature method was used as discussed in Ref. 8. The hot wires were calibrated by measuring their total voltage at different dynamic pressures between 0 and 8.0 inches of water. This calibration was done at three free-stream temperatures, 72°, 84°, and 92°F to see how the calibrations were effected by temperature. By measuring the total voltage E and the RMS voltage $\overline{e'^2}$ the axial turbulence could be obtained from the relation

$$\frac{\sqrt{\overline{u'^2}}}{U} = \frac{2E\sqrt{\overline{e'^2}}}{n(E^2 - E_o^2)}$$

where n = .45 for Re < 44 based on the diameter of the hot wire, and E_o is the total voltage reading of zero velocity. Also by using the calibration curves the mean axial velocity could be found and compared with the mean velocity obtained from the pressure probe. To obtain the radial turbulence the following relation was used

$$\sqrt{\overline{(e_1' + e_2')^2}} = 2\left(\frac{1}{K}\right)\sqrt{\overline{v'^2}}$$

where $\overline{e_1'}$ and $\overline{e_2'}$ are the voltage fluctuations from the two cross-wires and K is the ratio of voltage to velocity obtained from the calibration curves. The radial shear stress was obtained directly from the uv correlator.

III. RESULTS

Since the sail of the model as well as the effect of pitch angle was to induce asymmetrics in the wake it was necessary to probe the entire wake structure. For this reason all of the profiles presented extend from one edge of the wake to the other or in the case of the vertical traverse, from the edge of the wake into the wake region of the sail.

The mean axial velocity, static pressure, and flow angularity is plotted for both $\alpha_e = 0°$ and $-2°$ at stations Z/D = 2, 10, and 40. The axial and maximum radial turbulence intensity and maximum radial shear stress was also plotted for the same angles and stations.

First consider the results for the model at $\alpha_e = 0°$. In the near wake (Z/D = 2) there is a momentum defect at the center of the wake and then a momentum excess region in the outer portion of the wake. The static pressure decreases in the wake of the propeller as in the case of a swirling vortex. The propeller swirl is indicated by examining the flow angularity. For the horizontal profiles, large variations in flow pitch are measured with very small changes in the flow yaw, but in the vertical profiles the substantial flow angularity is in the yaw direction (Fig. 15, 16).

At Z/D = 10 the momentum excess and defect regions have decreased and spread out. The static pressure variation has also decreased and the swirl has decreased to the point that the flow angularity is only half the value measured at Z/D = 2 (Fig. 17).

By Z/D = 40 there is only a small momentum excess in the wake and its character is very similar to the far wake of a jet zero-momentum (Refs. 1 and 2). The static pressure is uniform across the wake and the swirl has completely diminished as seen by the small flow angularity (Fig. 18, 19).

The axial turbulence intensity is characterized by a highly fluctuating nature in the near-wake (Z/D = 2). At this station the velocity fluctuations are up to 10% of the free-stream velocity in the center of the wake (Fig. 20). At Z/D = 10 the turbulence intensity has decreased to about 6% of the free-stream velocity and does not vary significantly across the wake (Fig. 22). The radial turbulence intensity is somewhat larger than the axial intensity but follows the same trends. As is expected, the maximum shear stress occurs in the region of the greatest velocity gradient. This is especially obvious at the Z/D = 2 station.

The effect of the sail on the mean flow and turbulence quantities is seen in the vertical profiles at each station. The sail produces a larger momentum deficit in the upper portion of the vertical profile which indicates the increased drag on the body due to the sail (Fig. 23-26). The flow angularity is also reduced in the region behind the sail. This reduction is as much as 6.5° at Z/D = 2, (Fig. 16), and 3° at Z/D = 10, (Fig. 27). Also the static pressure is increased by the presence of the sail substantially. This increase is up to 50% higher in the upper portion of the vertical profile as compared to the lower portion (Fig. 16). The effect on axial turbulence intensity

was to increase the level of turbulence in the vertical profile behind the sail (Fig. 28, 29). Similarly the radial turbulence intensity was increased by the sail. The radial shear stress was also increased in the vertical profile behind the sail.

The results for the pitched condition shows increased asymmetries in the vertical profiles. The flow angularity is decreased in the upper region of the vertical profile by 9° at the Z/D = 2 station (Fig. 31) and by 6° at the Z/D = 10 station (Fig. 33). The static pressure is again higher above the wake center for the pitched configuration. The maximum turbulence intensity is increased by 15% at the Z/D = 2 station (Fig. 28) and by 5% at the Z/D = 10 station (Fig. 34). At 40 diameters the turbulence intensity and mean flow profiles are about the same for both the pitched and unpitched configurations (Fig. 36). The radial intensity again follows the same trends as the axial intensity. The maximum shear stress is also increased at stations Z/D = 2 and 10 for the pitch conditions while remaining about the same at Z/D = 40 (Fig. 38). The comparison of maximum turbulence intensity with previous work shows an increased turbulence level due to the higher propeller rpm needed to balance the extra drag of the sail (Fig. 39).

IV. CONCLUSIONS AND RECOMMENDATIONS

From the results presented several conclusions about the effects of appendages and non-zero pitch angles on the wake structure of a propeller driven body can be asserted.

First an appendage such as a submarine sail reduces the propeller swirl in the region subjected to the wake of the sail. This decrease in swirl causes an increase in static pressure as would be seen in a vortex of decreasing strength. The axial turbulence intensity is increased by the value of the sail induced turbulence at each station. This suggests that the turbulence in the wake of an appendage might be super-imposed on the turbulence profile of the main body.

Second the pitched condition further reduces the swirl and increases the static pressure in the region behind the sail. These effects are primarily confined to the vertical plane and little change in the horizontal profiles is seen. The maximum turbulence intensity in the wake up to Z/D = 10 is increased for the pitch condition. However, by 40 diameters the turbulence levels are equivalent for both the pitched and unpitched conditions.

Third, the effect of the sail on the drag coefficient is to increase it from C_D = .092 as calculated for the body without sail by Swanson[4] to C_D = .19 with the sail. This large increase in C_D indicates the need for streamlining of such appendages on slender axisymmetric bodies.

From this experimental work further work is suggested in analyzing the turbulent shear stress $\overline{u'v'}$ and the $\sqrt{v'^2}$, $\sqrt{\omega'^2}$ turbulence intensities. Due to the large swirl in the near wake, the cross-wire measurements of radial turbulence intensity and radial shear stress may have been substantially effected. Higher quality measurements of such quantities may require the use of more sophisticated equipment such as laser anemometers, or the tedious technique of aligning the cross-wire probe with the flow direction at each point.

REFERENCES

1. Ridjanovic, M., "Wake With Zero Change of Momentum Flux," Ph.D. Dissertation, 1963, University of Iowa, Iowa City, Iowa.

2. Naudascher, E., "Flow in the Wake of a Self-Propelled Body and Related Sources of Turbulence," Journal of Fluid Mechanics, Vol. 22, 1965, pp. 625-656.

3. Gran, R. L., "An Experiment on the Wake of a Slender Propeller-Driven Body," TRW Report 20086-6006-RU-80.

4. Swanson, R. C., Jr., Schetz, J. A., Jakubowksi, A. K., "Turbulent Wake Behind Slender Bodies Including Self-Propelled Configurations," VPI-AERO-024, 1974. (Available thru D.D.C.)

5. Chieng, C. C., Jakubowski, A. K. Schetz, J. A., "Investigation of the Turbulent Properties of the Wake Behind Self-Propelled, Axisymmetric Bodies," VPI-AERO-025, 1974. (Available thru D.D.C.)

6. Winternitz, F. A. L., "Probe Measurements in Three-Dimensional Flow," Aircraft Engineering, August 1956, p. 273.

7. Mason, W. H. and Marchman, J. E., III, "Fairfield Structure of an Aircraft Trailing Vortex, Including Effects of Mass Injection," NASA CR-62078, 1972.

8. Hinze, J. O., Turbulence--An Introduction to Its Mechanism and Theory, McGraw-Hill, New York, 1959.

9. Birkhoff, G. and Zarantonello, E. H., Jets, Wakes, and Cavities, Academic Press, New York, 1957.

10. Houghton, E. L. and Brock, A. E., Aerodynamics for Engineering Students, St. Martin's Press, New York, 1970.

11. Hall, A. A. and Hislop, G. S., "Velocity and Temperature Distributions in the Wake Behind a Heated Body of Revolution," Proc. Comb. Phil. Soc. 34, 1938.

12. Cooper, R. D. and Lutzky, M., "Exploratory Investigation of the Turbulent Wakes Behind Bluff Bodies," DTMB R4D Rept. No. 953, October 1955.

13. Ilizorova, L. I. and Pochkina, K. A., "Experimental Study of a Wake Behind a Body of Revolution," Prom. Aerodynamika, No. 23, 1962.

14. Carmody, Thomas, "Establishment of the Wake Behind a Disk," Journal of Basic Engineering-Transactions of the ASME, December 1964.

15. Wang, H., "Flow Behind a Point Source of Turbulence," Ph.D. Dissertation, 1963, University of Iowa, Iowa City, Iowa.

16. Ginevskii, A. S., Pochkina, K. A., and Ukhanova, L. N., "Propagation of Turbulent Jet Flow with Zero Excess Momentum," Fluid Dynamics Academy of Sciences USSR, Vol. 1, No. 6, November-December 1966, Faraday Press, Inc.

17. Buckinskaya, E. K. and Pochkina, K. A., "Investigation of Vortex Wake Behind a Body of Revolution," Prom. Aerodynamika No. 23, 1962.

18. Chevray, R., "The Turbulent Wake of a Body of Revolution," Journal of Basic Engineering-Transactions of the ASME, Series D, 1968.

19. Bukreev, V. I., Kostomakka, V. A., and Lytkin, Yu, "Axisymmetric Turbulent Wake Behind a Streamlined Body," Siberskae, Otdeline An SSSR, Institut Gidrodinamiki, Dinamika Splashhoi Sredy, No. 10, 1972.

20. Hokenson, G. J. and Schetz, J. A., "Free Turbulent Mixing in Axial Pressure Gradients," Journal of Applied Mechanics, June 1973.

21. Bukreev, V. I., Kostomakha, V. A., and Lytkin, Yu, M., "Turbulent Energy Balance in Axisymmetric Wakes Behind Differently Shaped Bodies," Prikladnaya Mikhanika i Tekhnicheskaya Fizeka, No. 1, 1974.

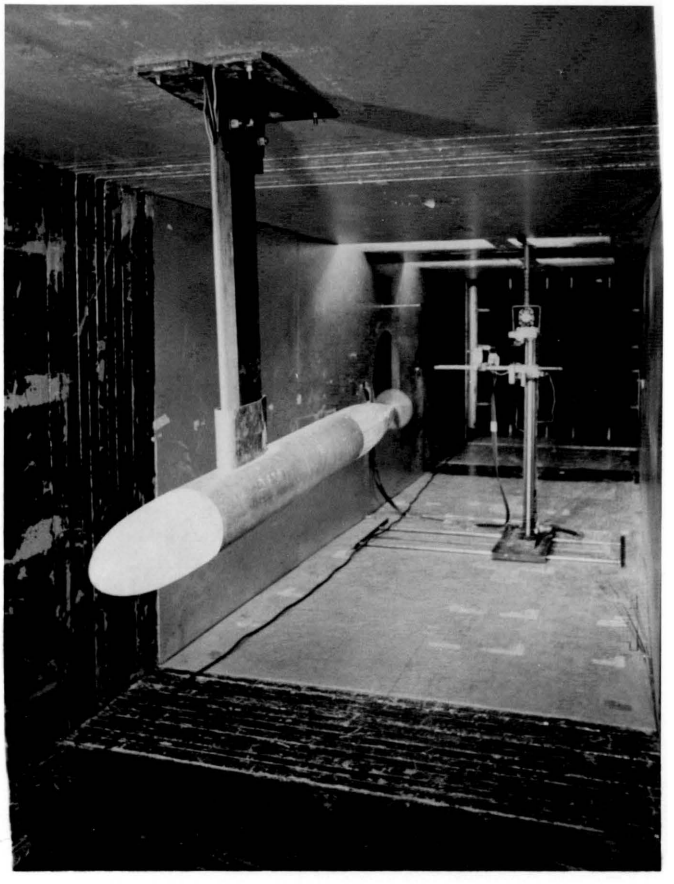

Fig. 1 PICTURE OF MODEL AND TRAVERSE

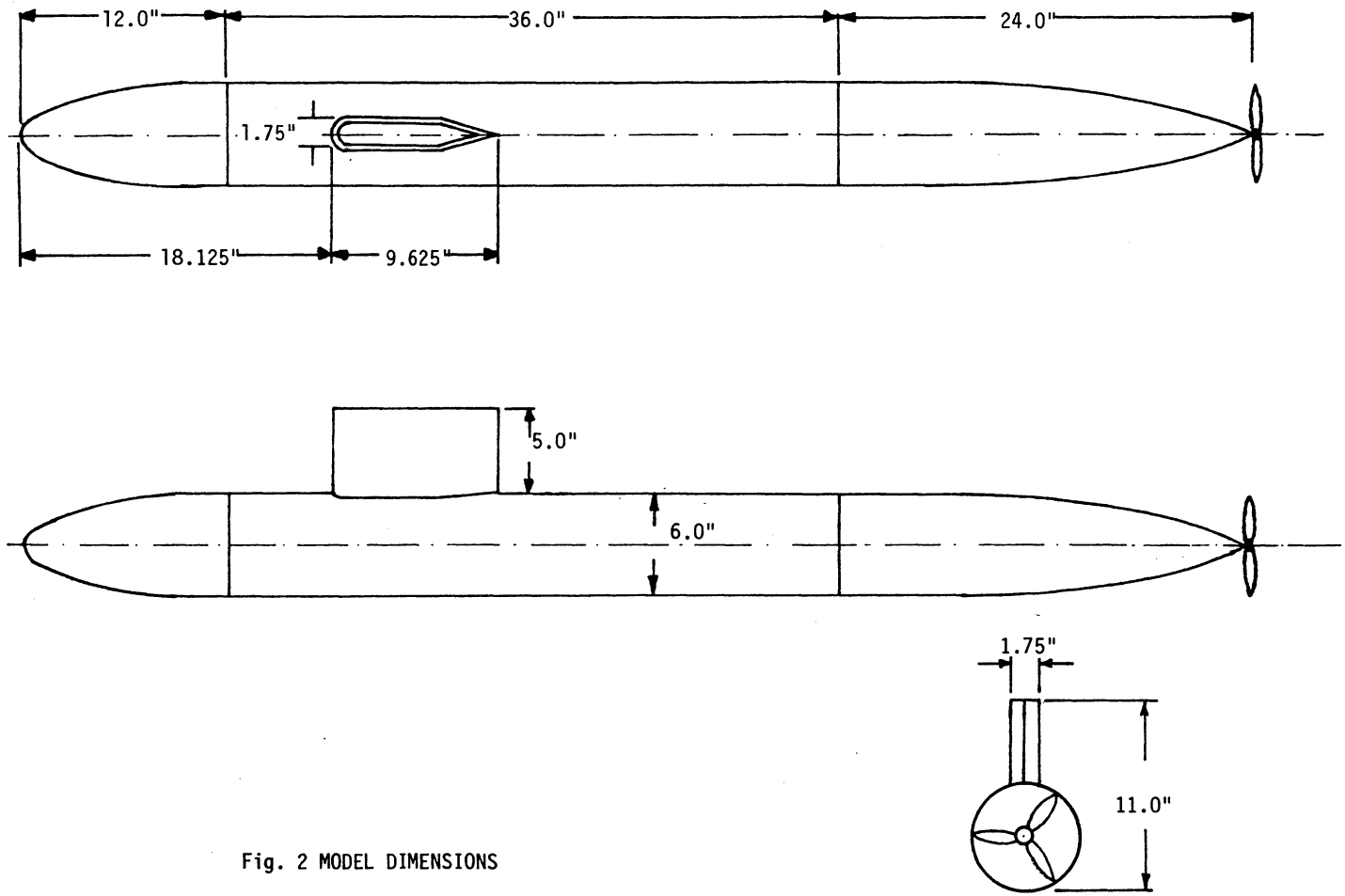

Fig. 2 MODEL DIMENSIONS

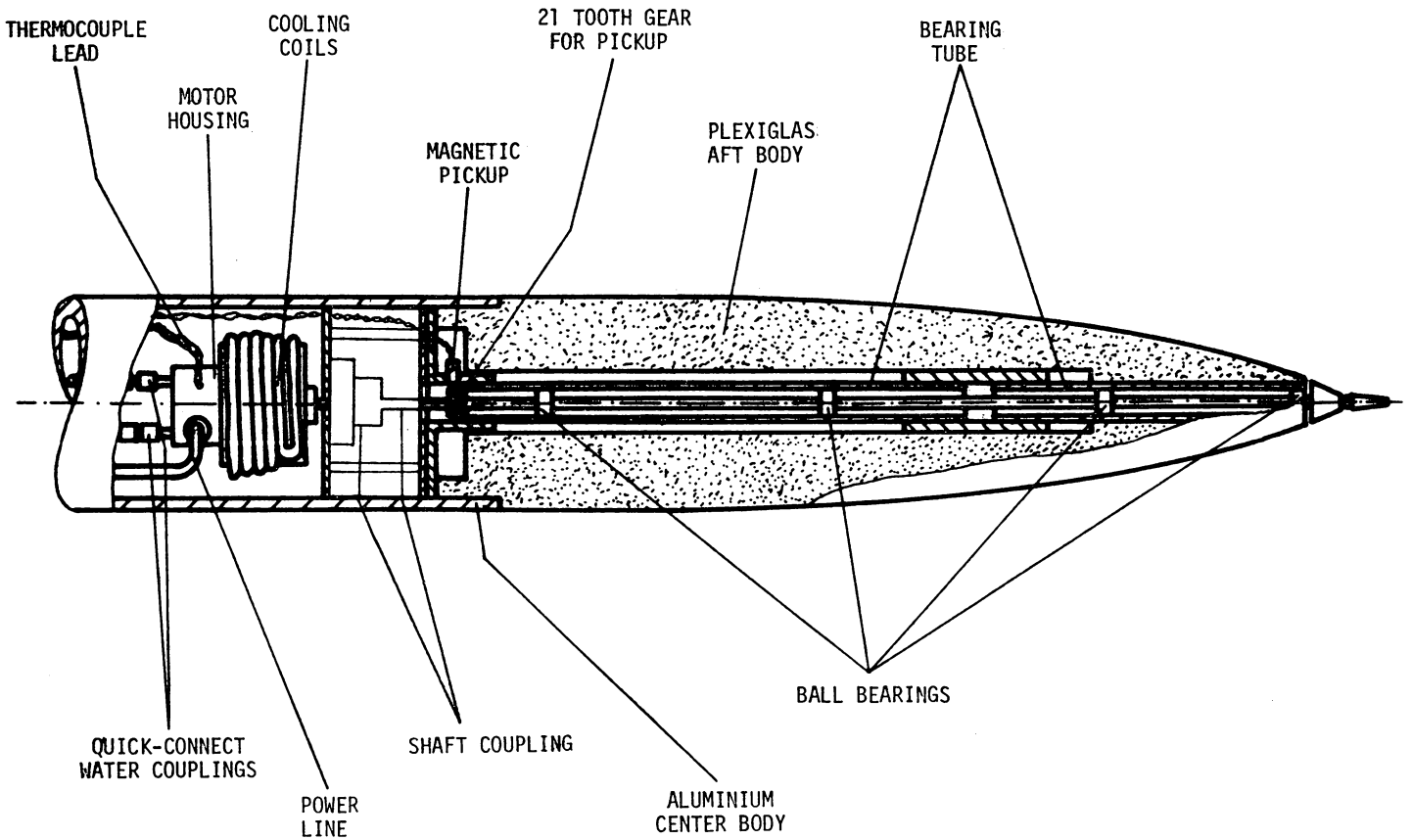

Fig. 3 MODEL TAIL SECTION

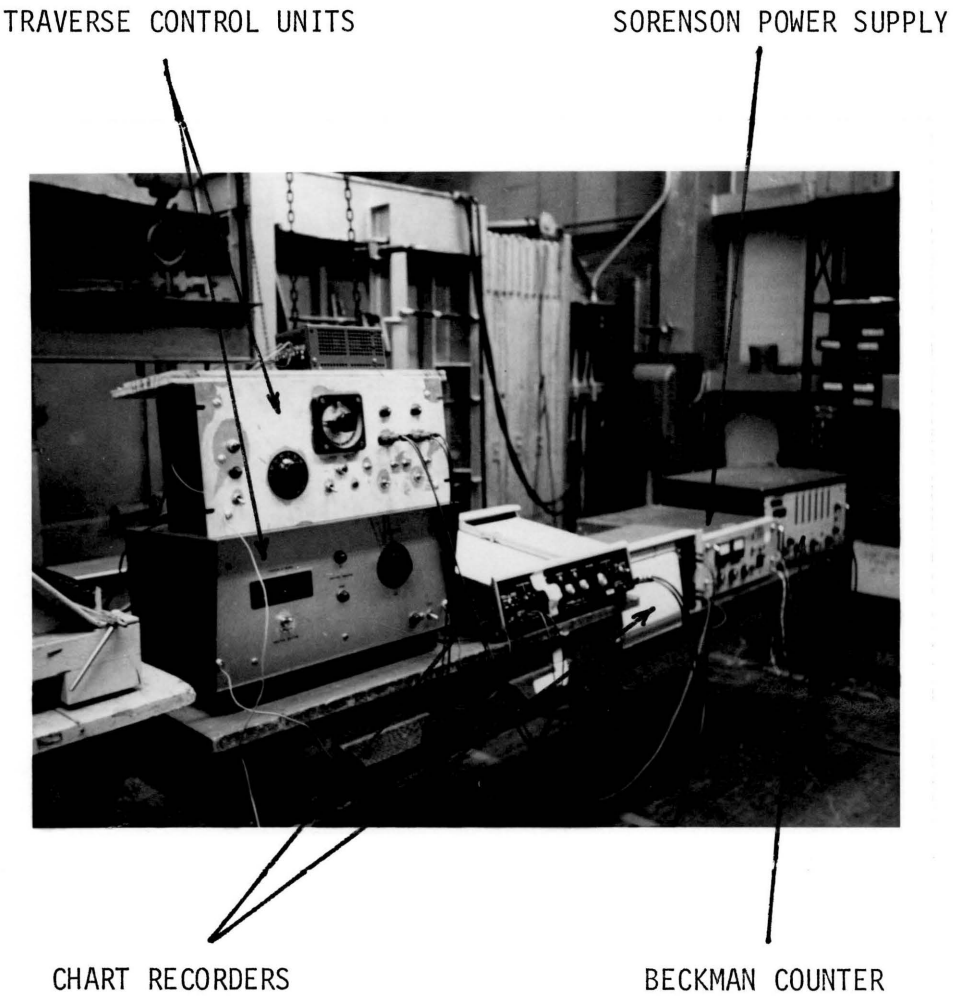

Fig. 4 PICTURE OF EXPERIMENTAL EQUIPMENT

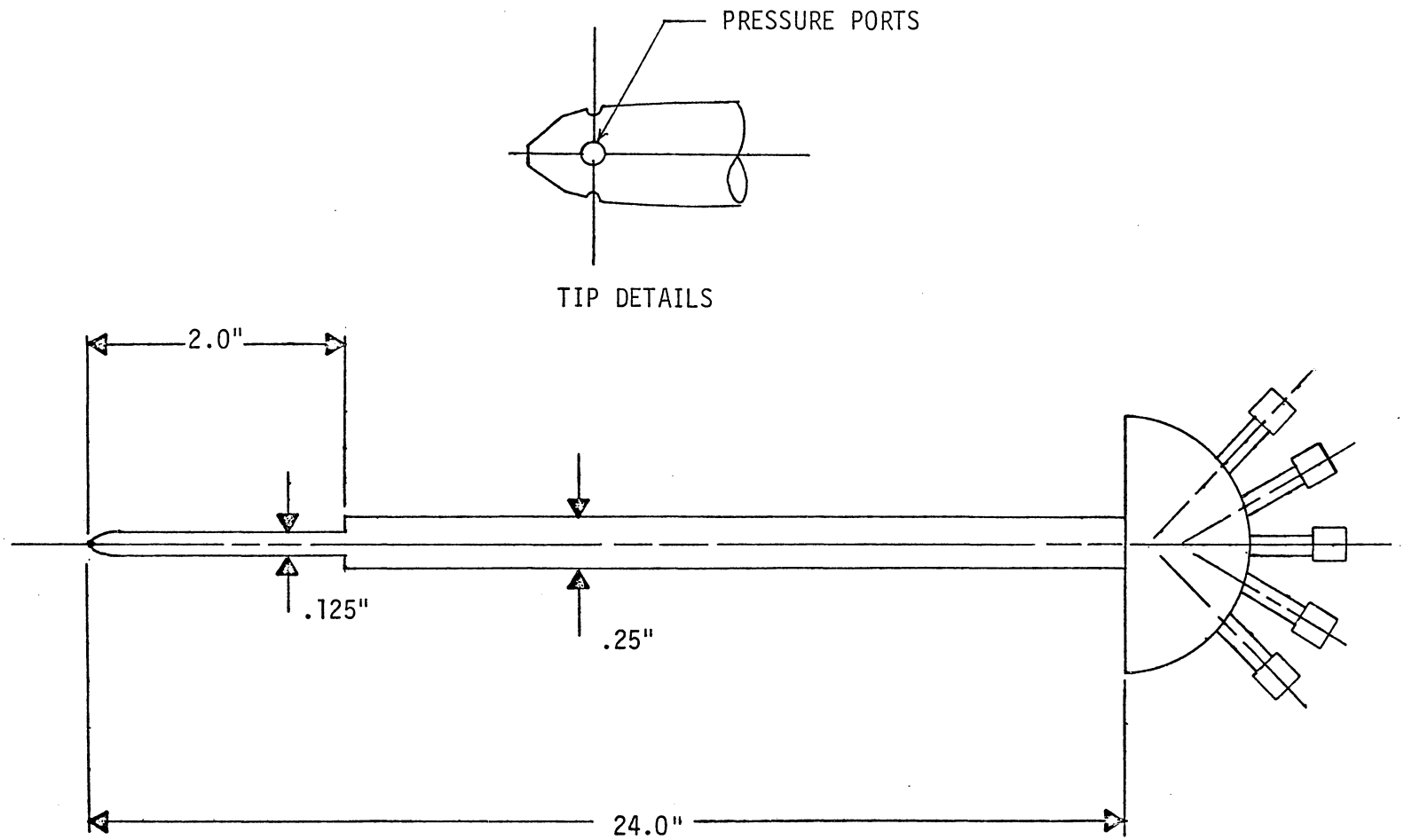

Fig. 5 YAWHEAD PROBE

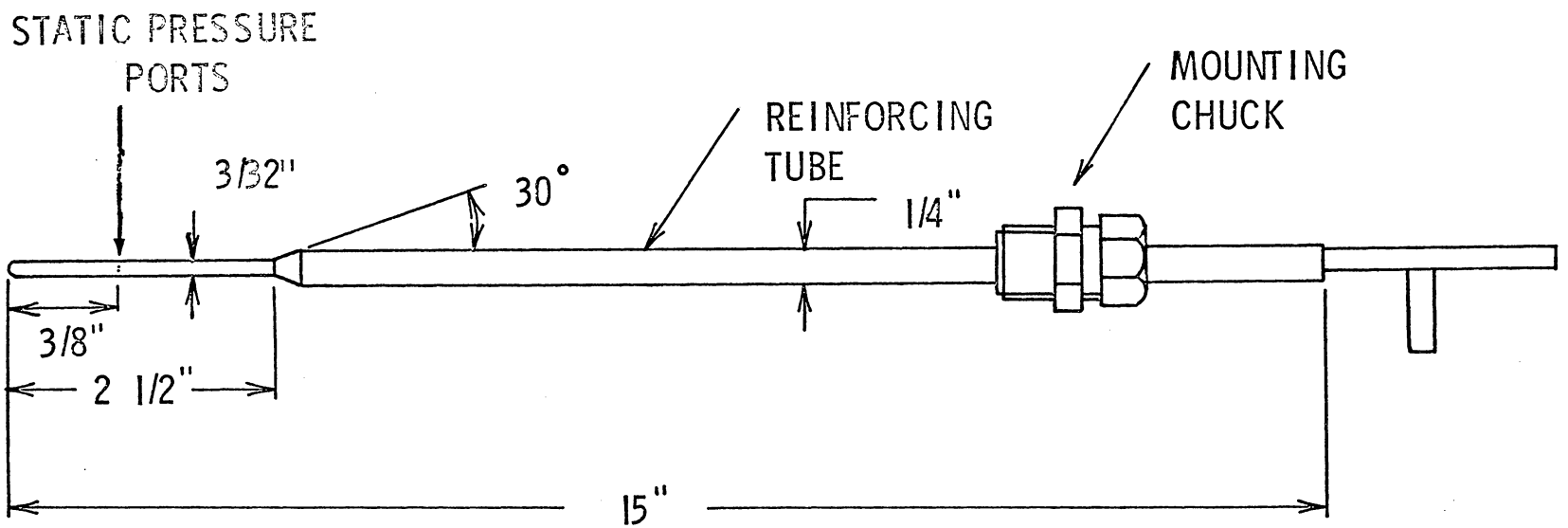

FIG. 6 PITOT-STATIC PROBE

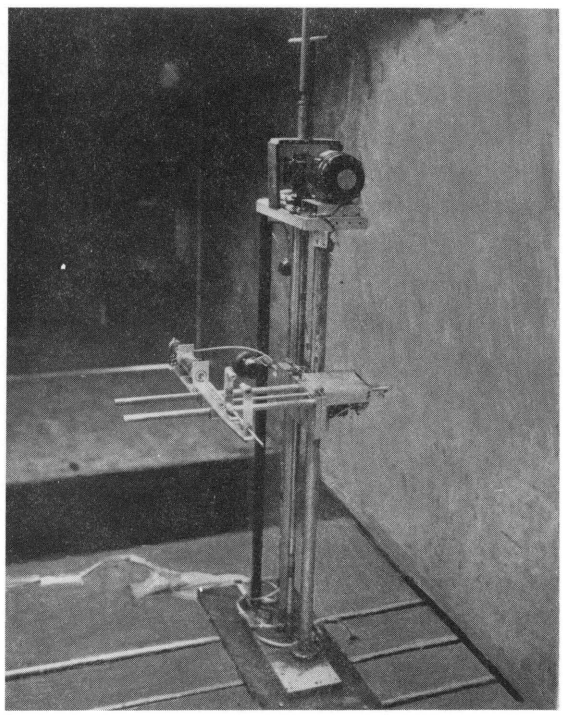

FIG. 7 AUTOMATIC TRAVERSE

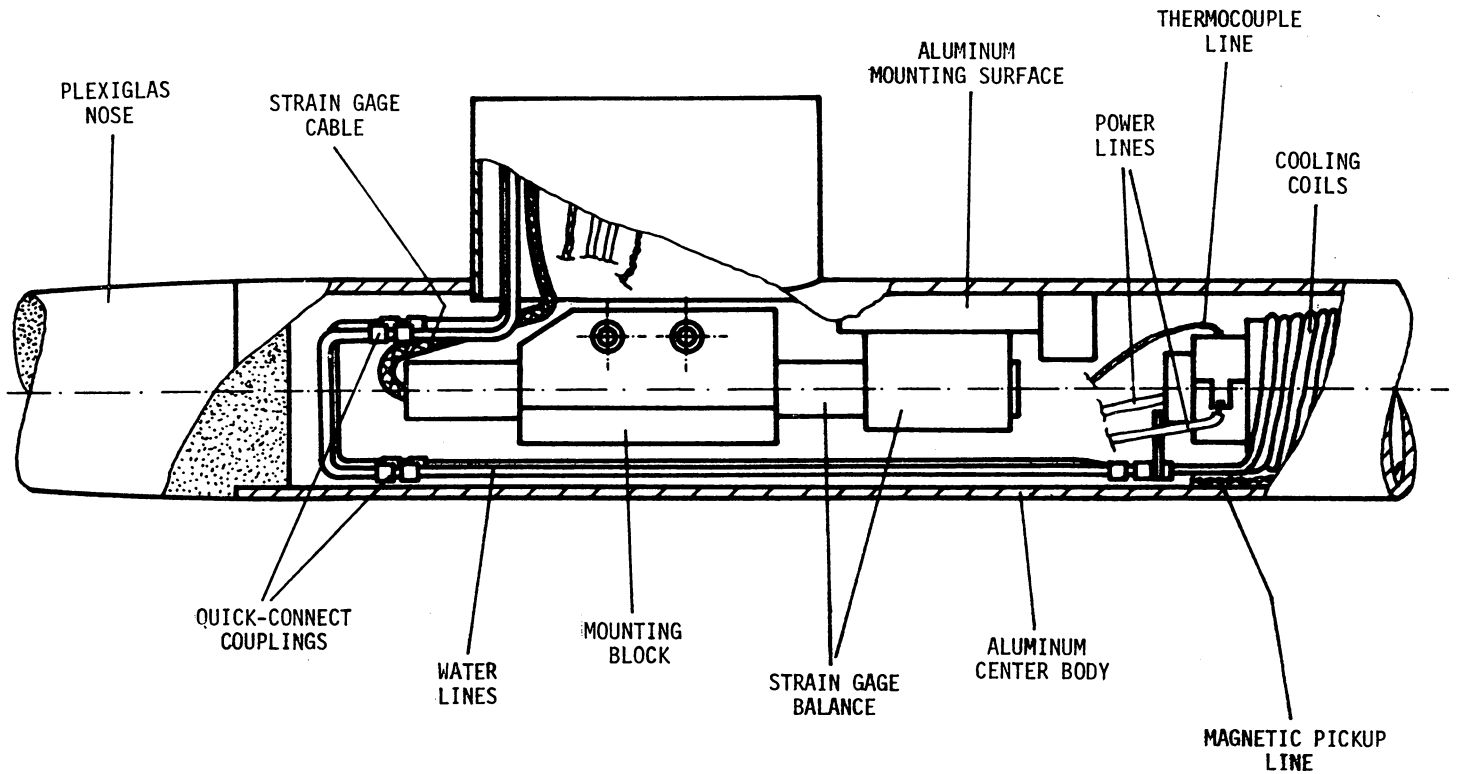

Fig. 8 DETAIL OF BALANCE IN CENTERBODY

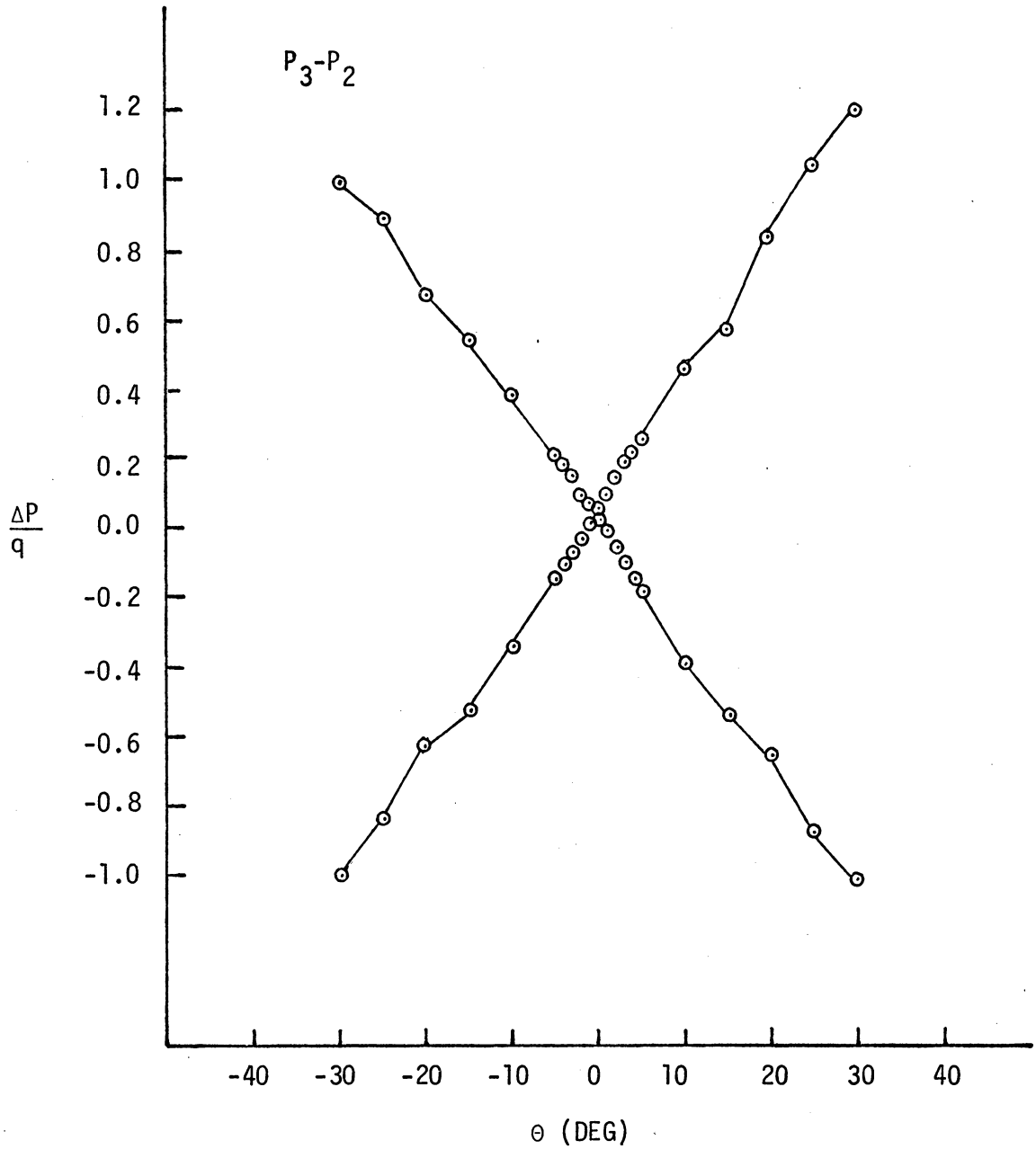

Fig. 9 YAW ANGLE CALIBRATION
FOR YAWHEAD PROBE

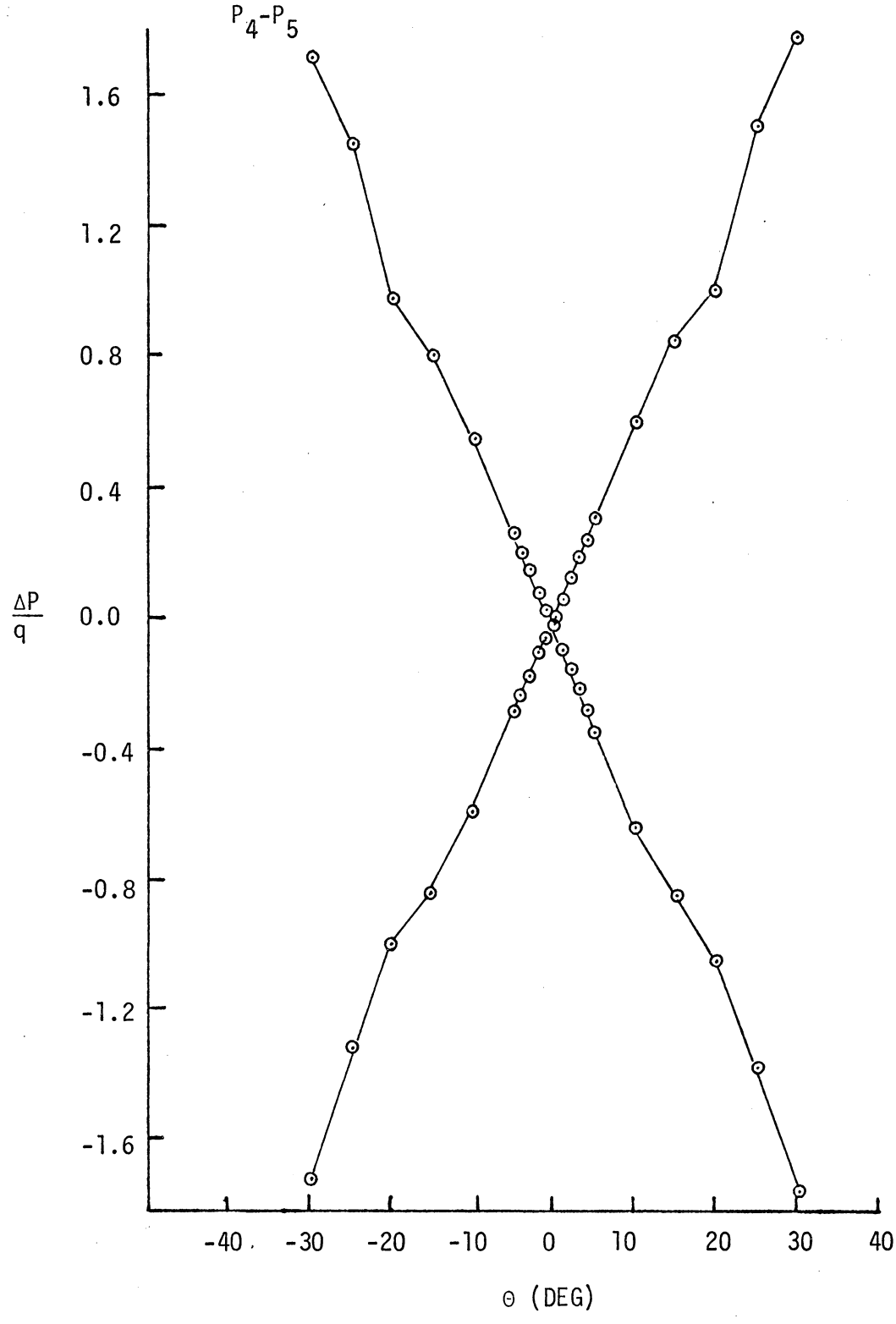

Fig. 10 PITCH ANGLE CALIBRATION
FOR YAWHEAD PROBE

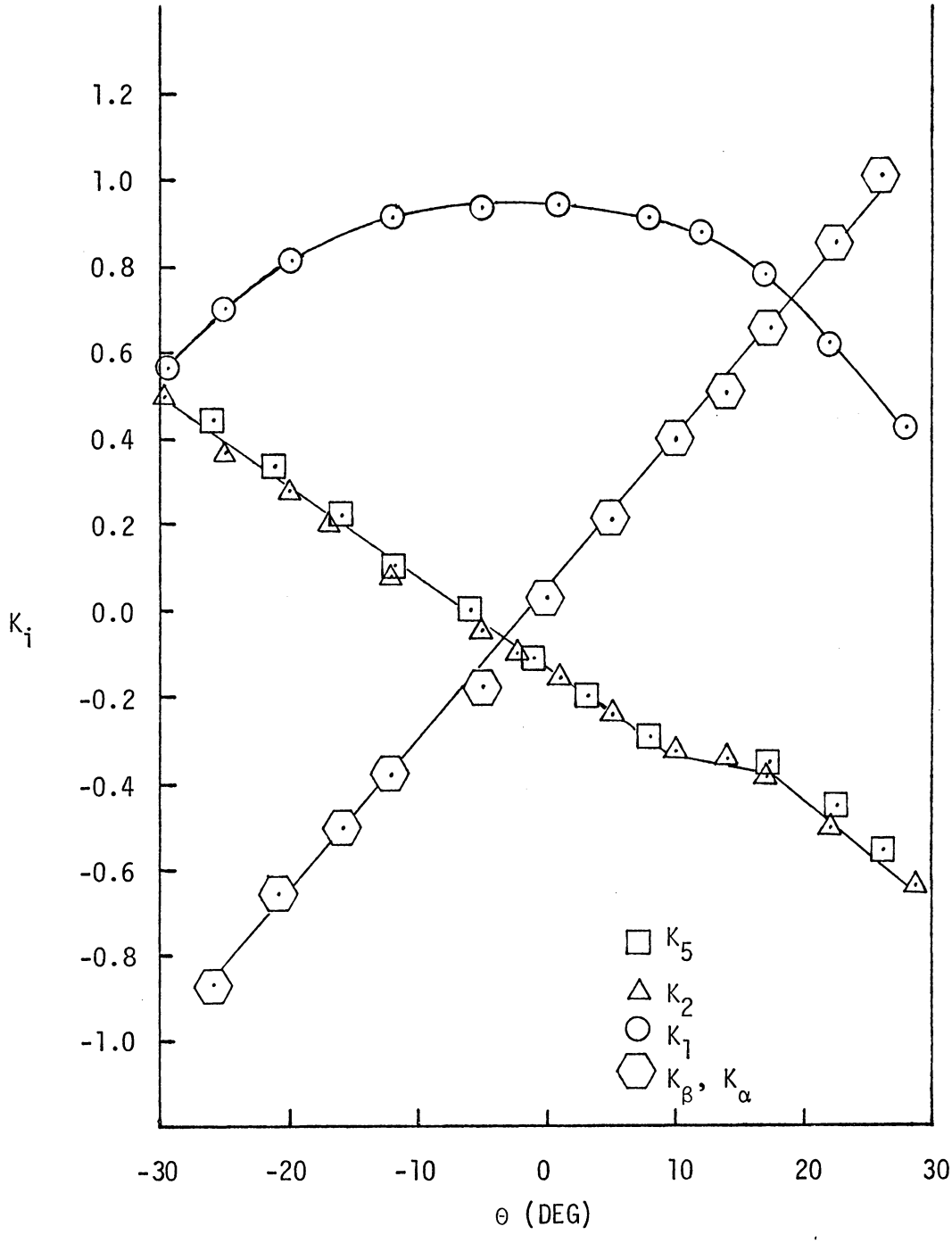

Fig. 11 CALIBRATION FOR STATIC PRESSURE FROM 3-D PROBE

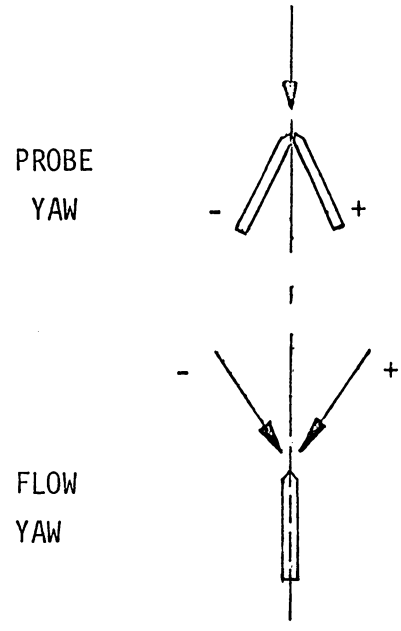

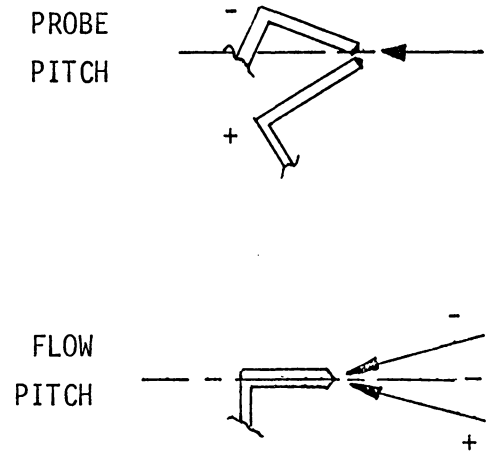

YAW ANGLE = PROBE YAW-FLOW YAW

PITCH ANGLE = PROBE PITCH-FLOW PITCH

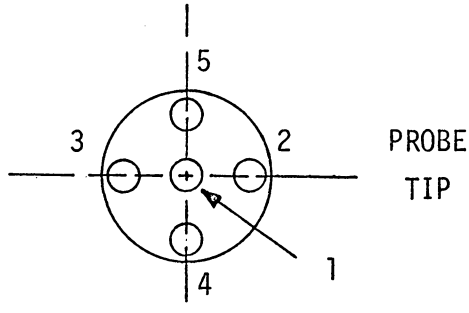

LOOKING DOWNSTREAM

Fig. 12 SIGN CONVENTIONS

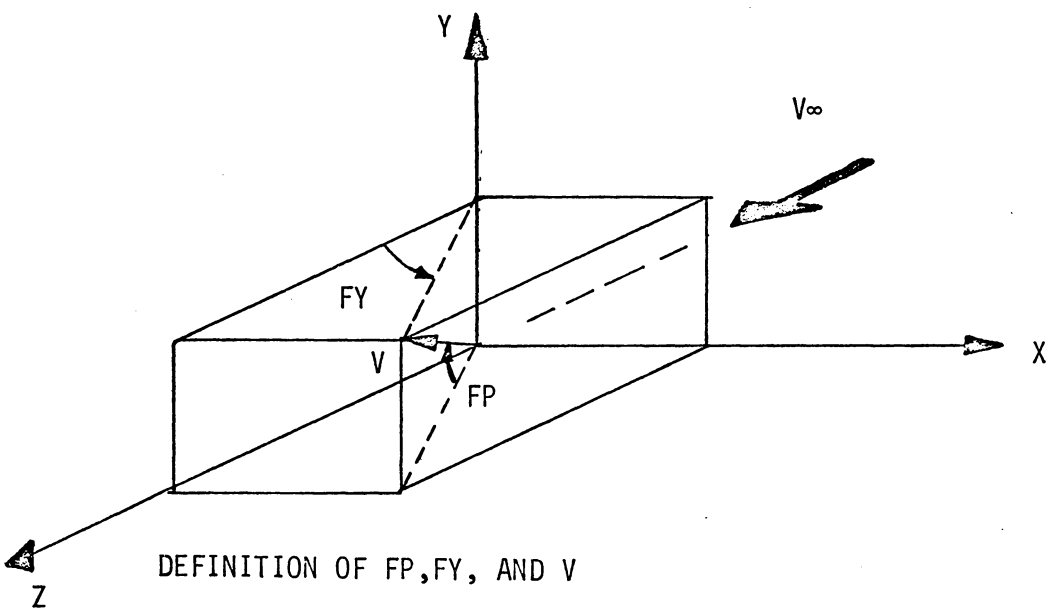

Fig. 13 COORDINATE SYSTEMS

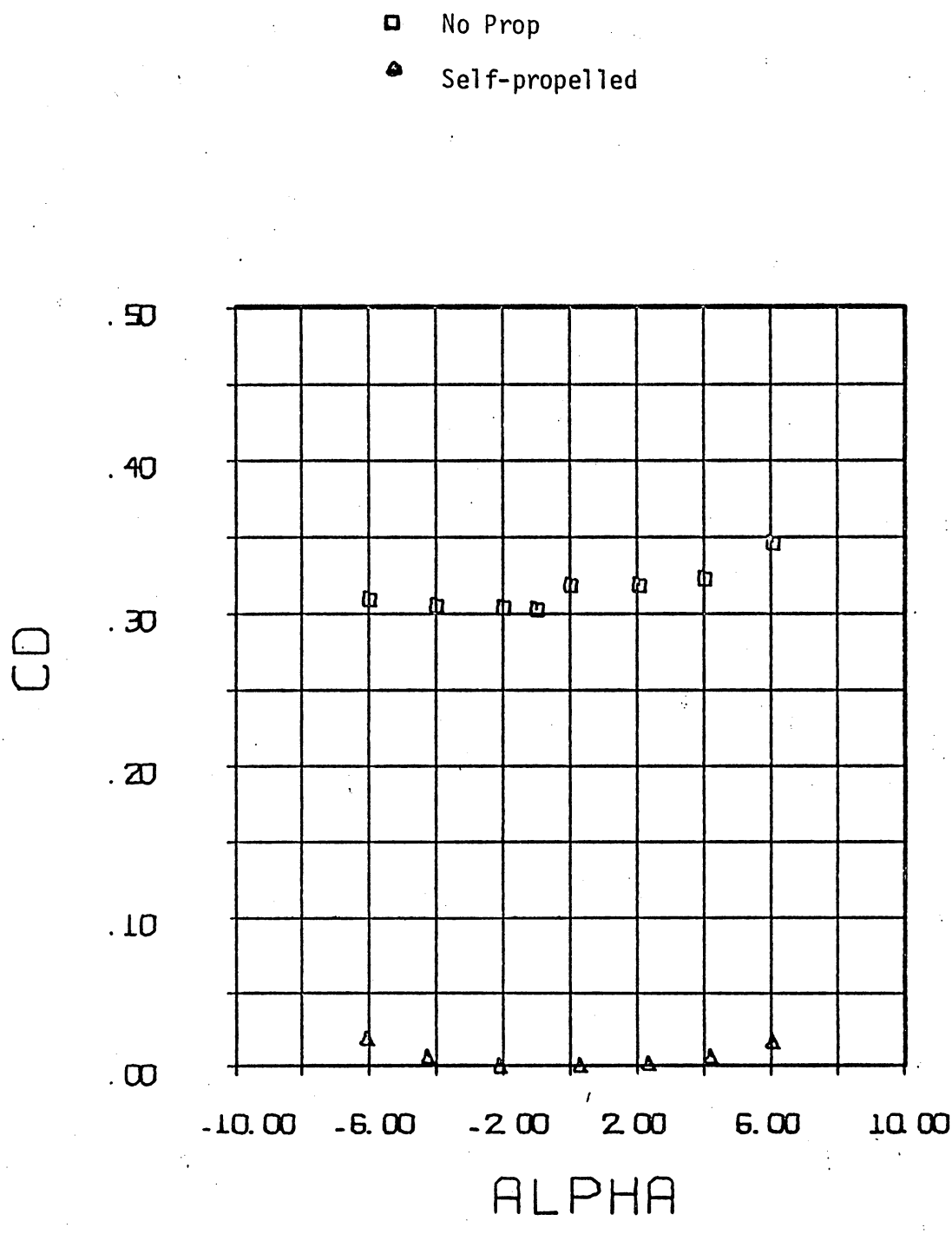

Fig. 14 C_D VERSUS PITCH ANGLE

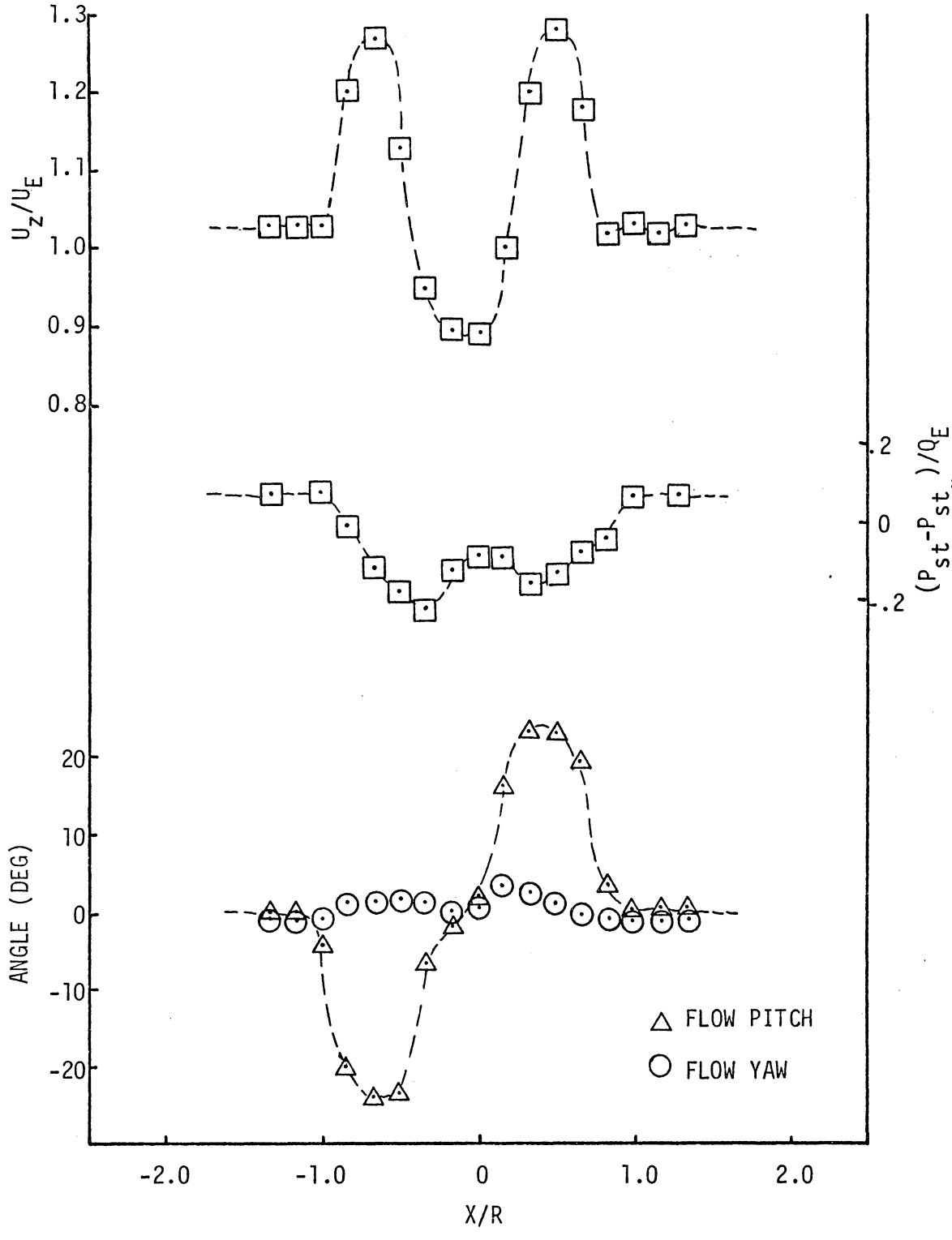

Fig. 15 MEAN AXIAL VELOCITY , FLOW ANGULARITY, AND STATIC PRESSURE HORIZONTAL PROFILE AT Z/D=2, Y/R=0, $\alpha_e=0^\circ$

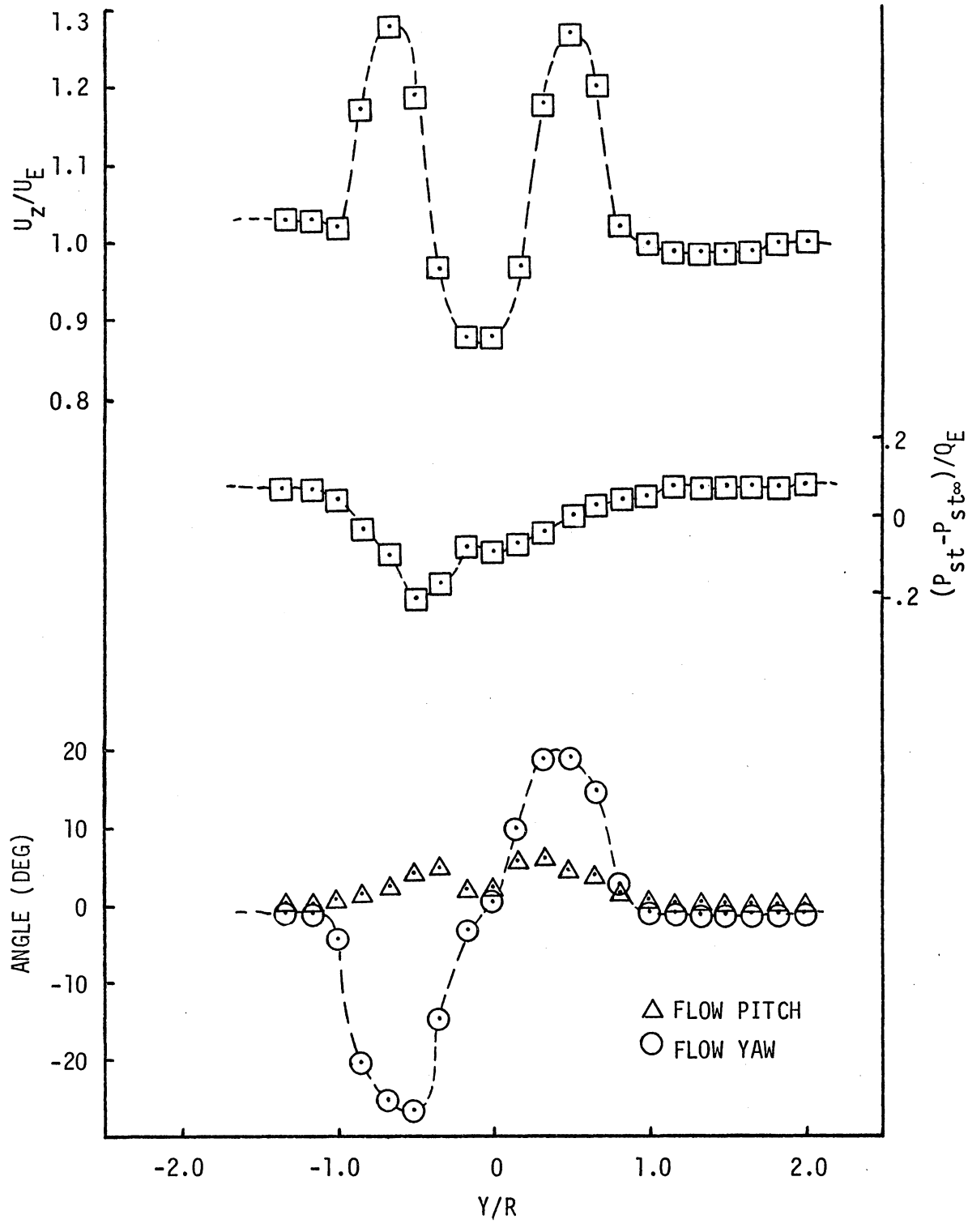

Fig. 16 MEAN AXIAL VELOCITY, FLOW ANGULARITY, AND STATIC PRESSURE VERTICAL PROFILE AT Z/D=2, X/R=0, $\alpha_e=0^o$

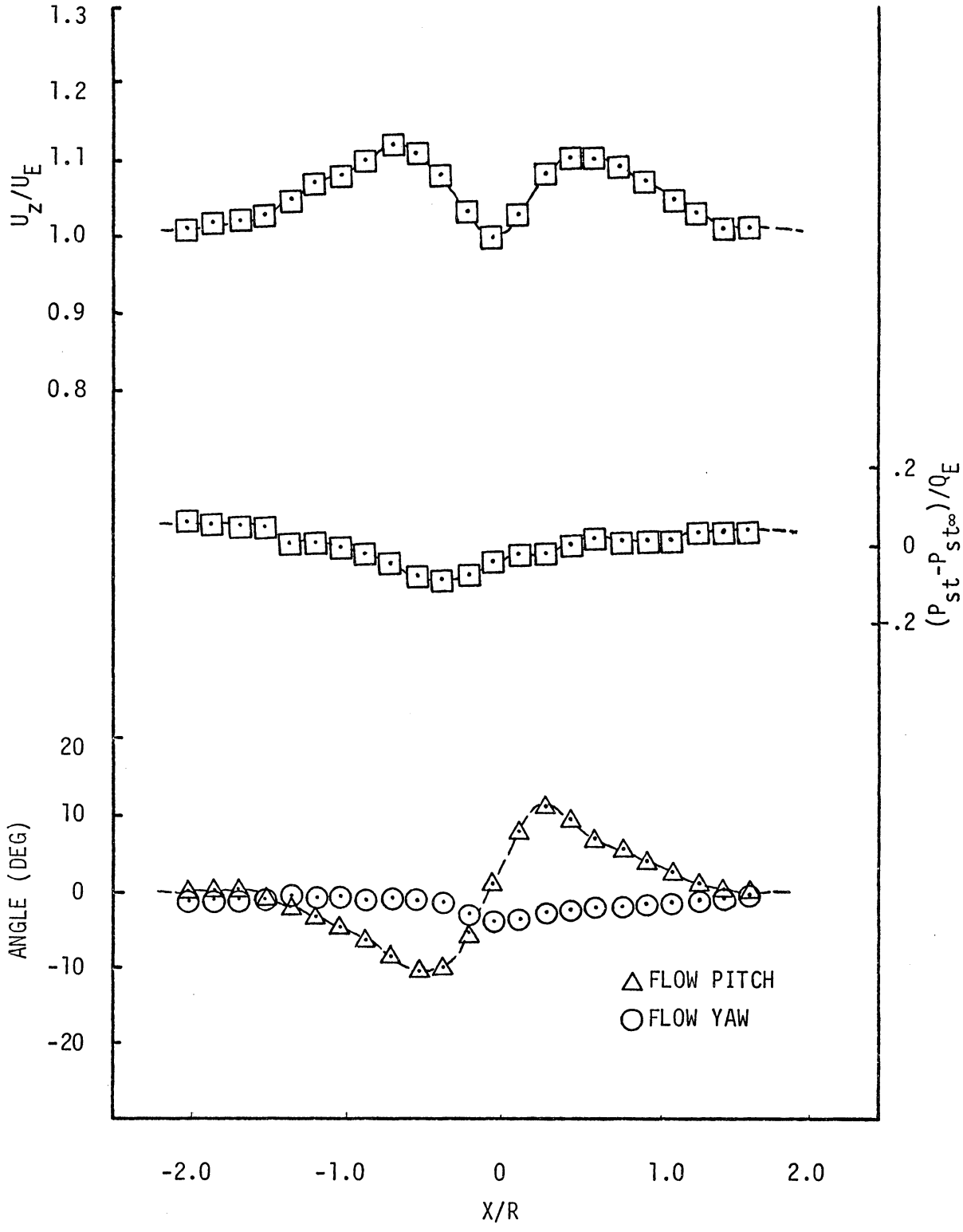

Fig. 17 MEAN AXIAL VELOCITY,FLOW ANGULARITY, AND STATIC PRESSURE HORIZONTAL PROFILE AT Z/D=10, Y/R=0, $\alpha_e=0^\circ$

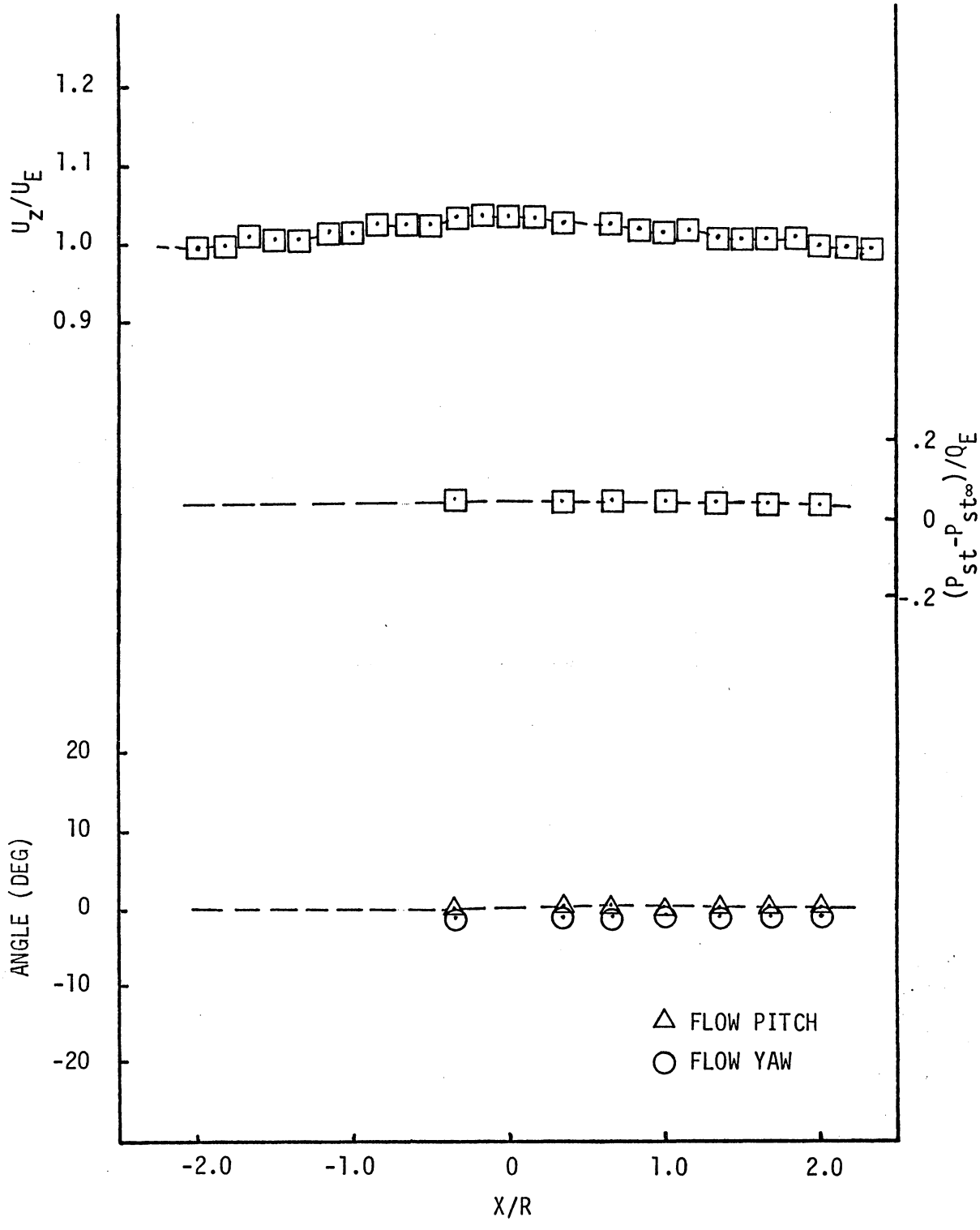

Fig. 18 MEAN AXIAL VELOCITY, FLOW ANGULARITY, AND STATIC PRESSURE HORIZONTAL PROFILE AT Z/D=40, Y/R=0, $\alpha_e=0^o$

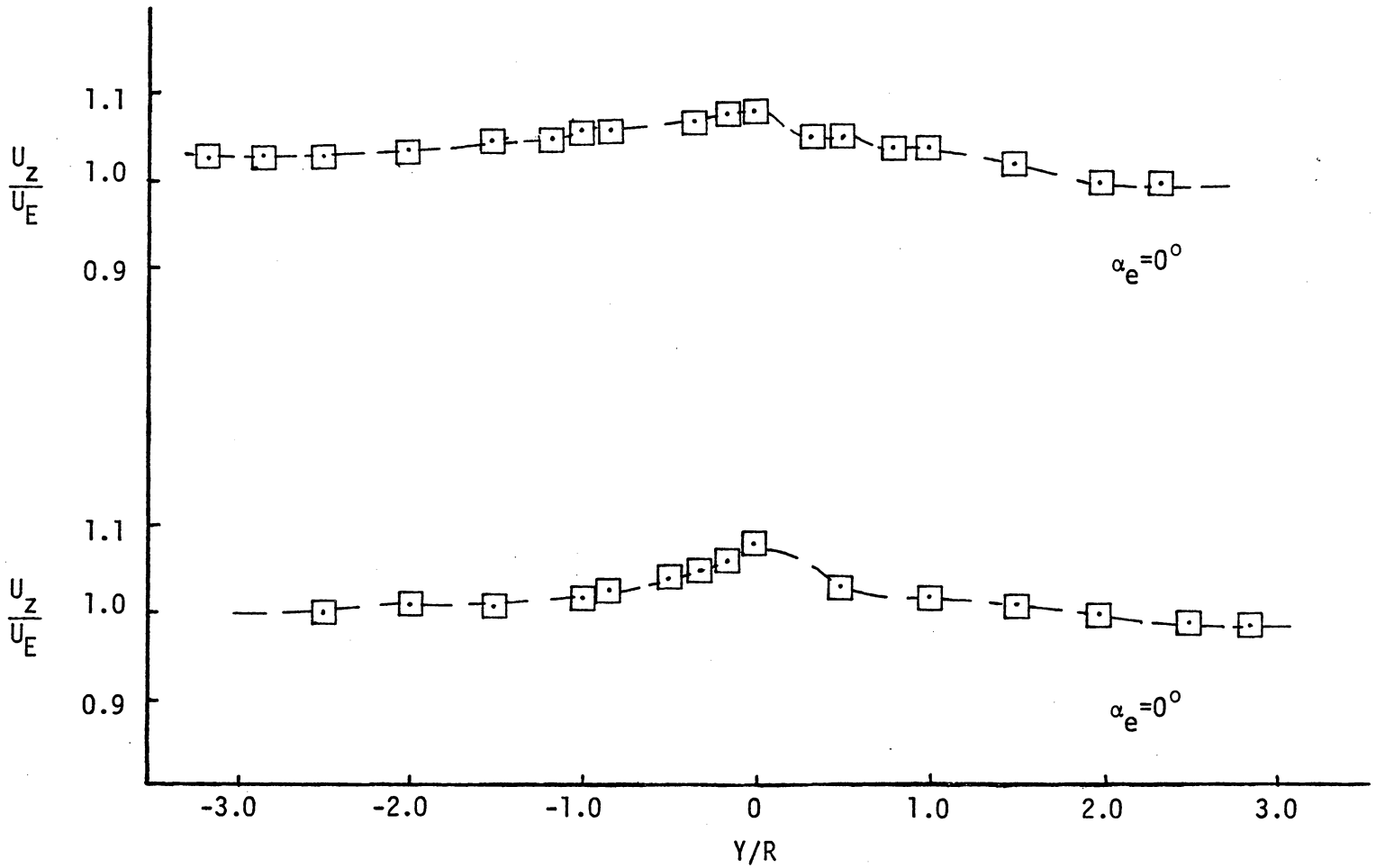

Fig. 19 MEAN AXIAL VELOCITY, VERTICAL PROFILES AT Z/D=40, X/R=0

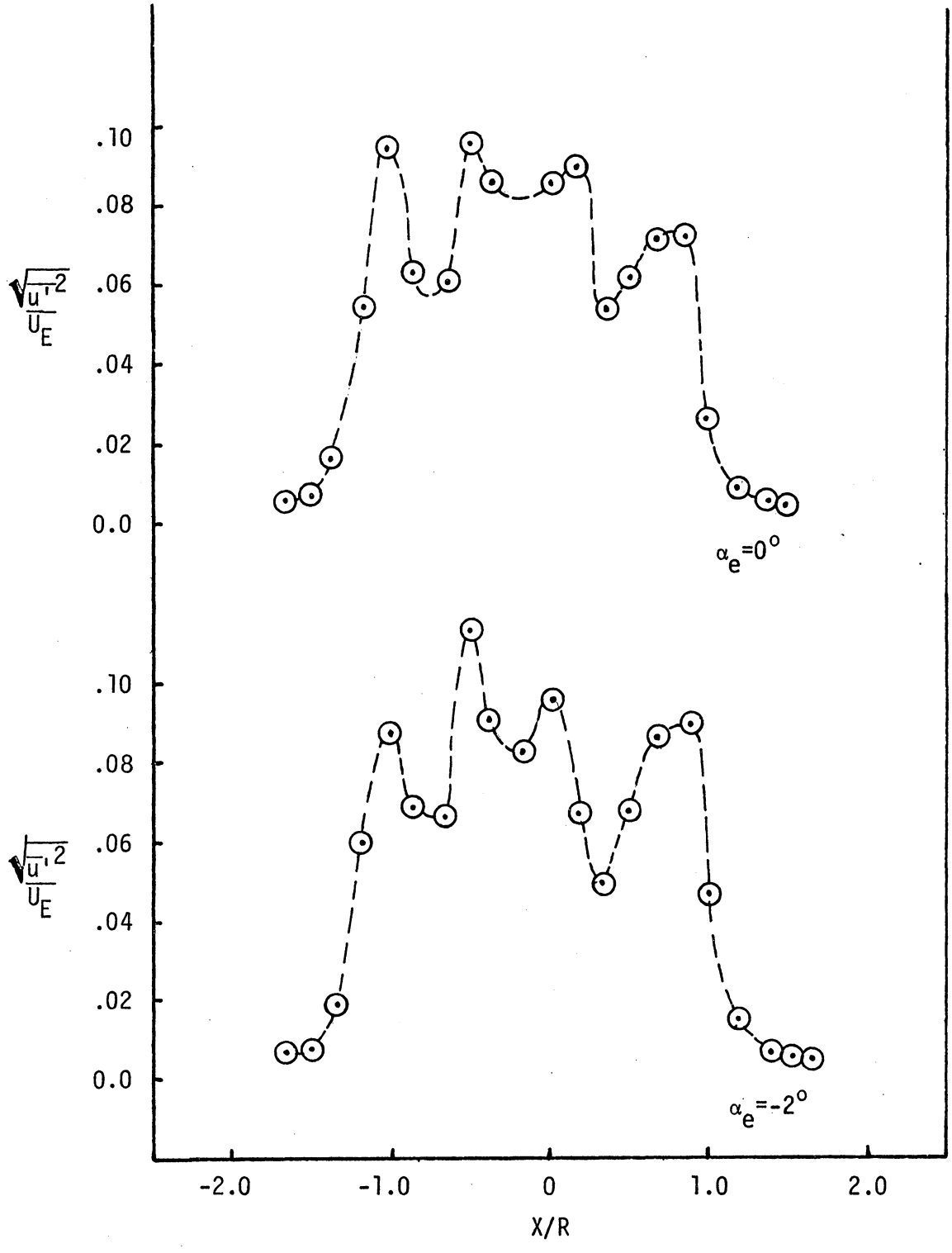

Fig. 20 AXIAL TURBULENCE INTENSITY HORIZONTAL PROFILE AT Z/D=2, Y/R=0

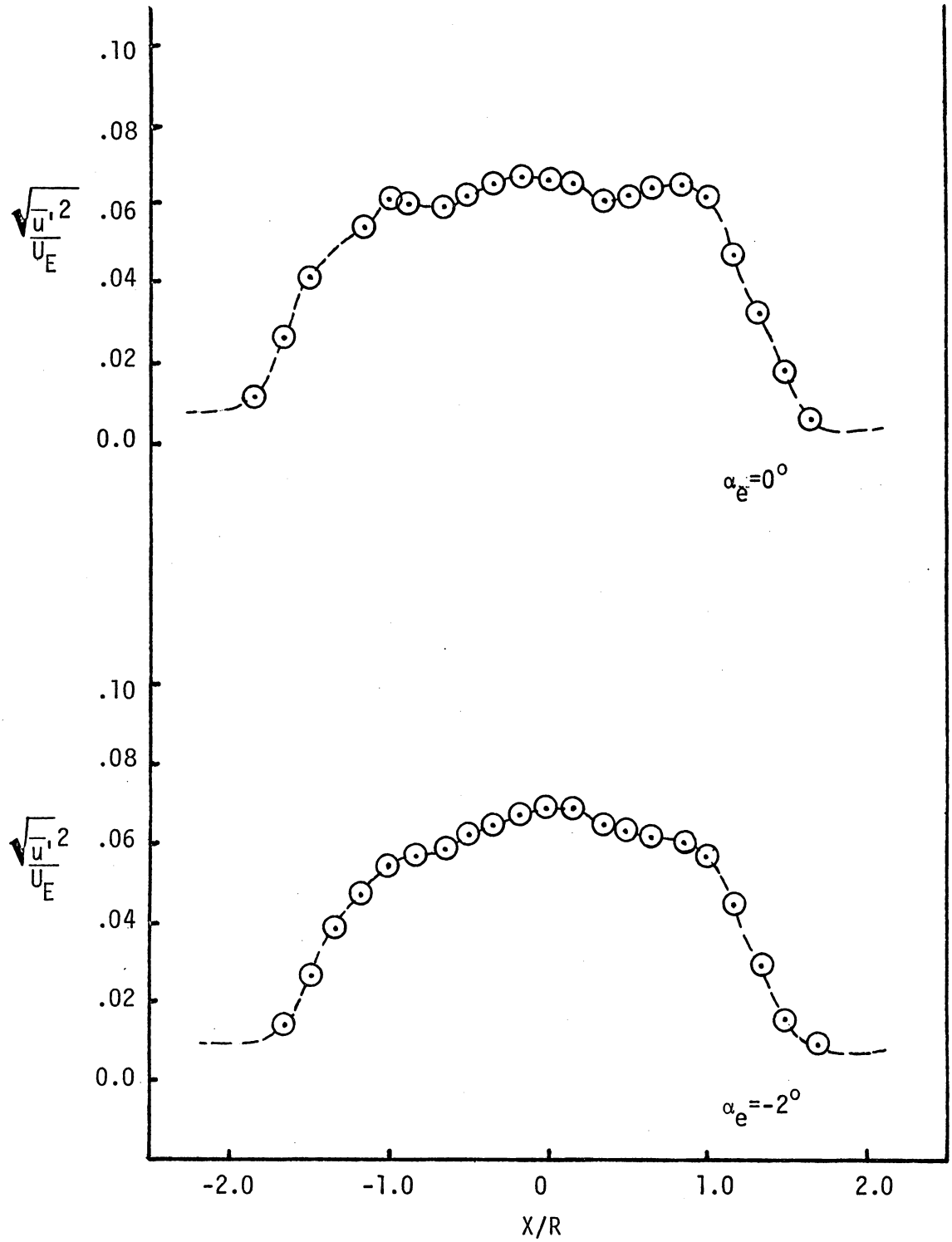

Fig. 21 AXIAL TURBULENCE INTENSITY HORIZONTAL PROFILE AT Z/D=10, Y/R=0

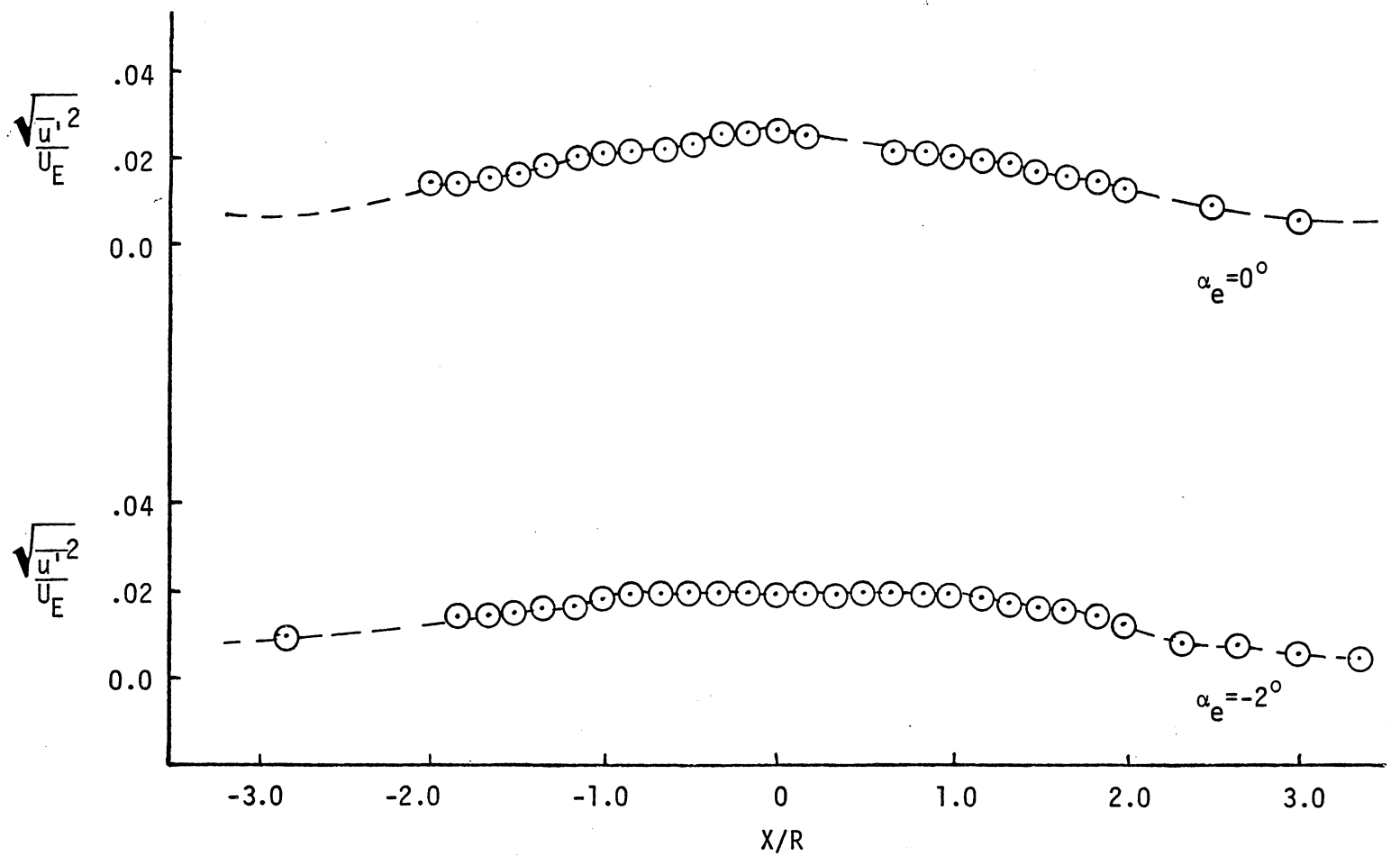

Fig. 22 AXIAL TURBULENCE INTENSITY HORIZONTAL PROFILE AT Z/D=40, Y/R=0

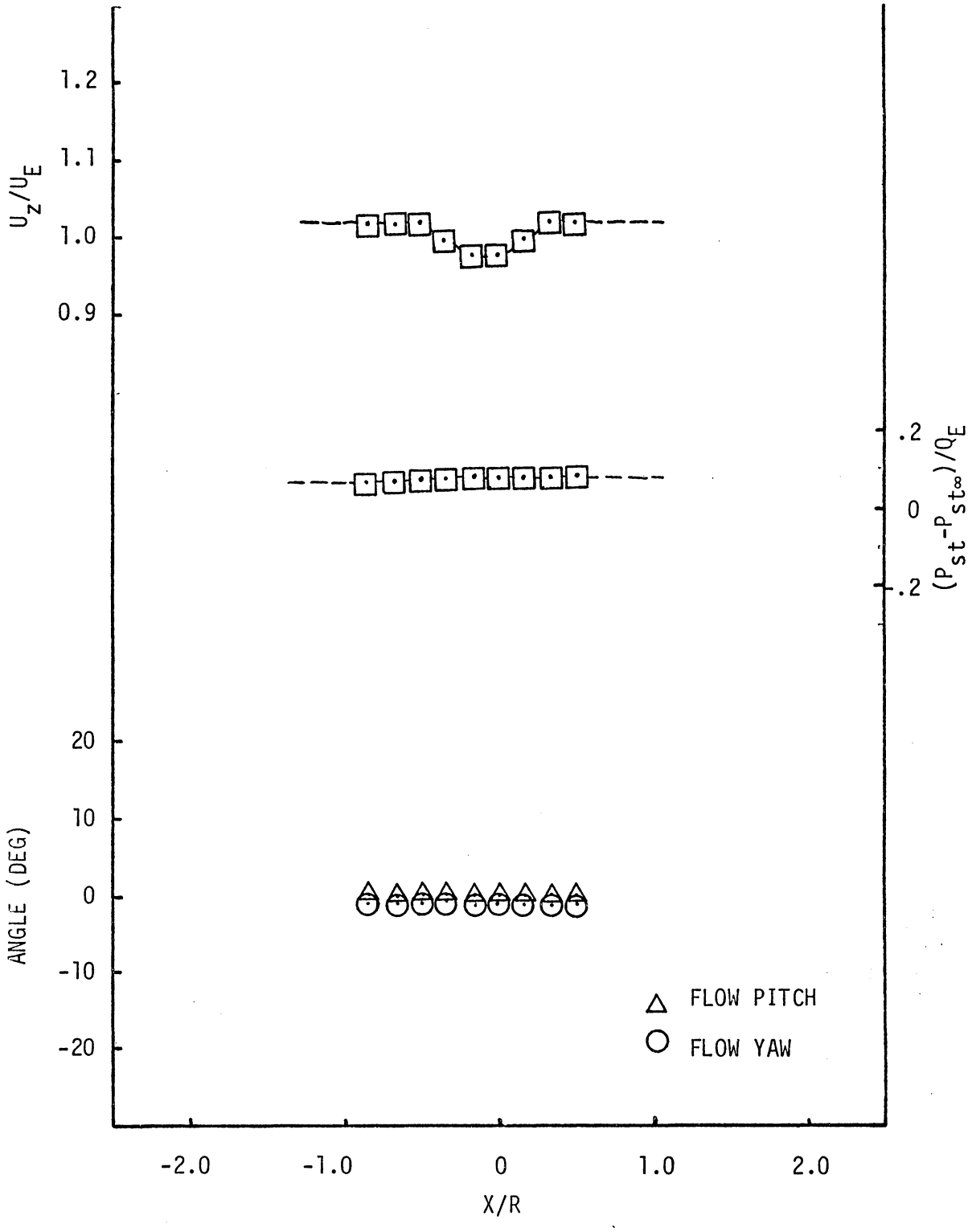

Fig. 23 MEAN AXIAL VELOCITY, FLOW ANGULARITY, AND STATIC PRESSURE ACROSS THE SAIL WAKE AT Z/D=2, Y/R=1.67, $\alpha_e=0^o$

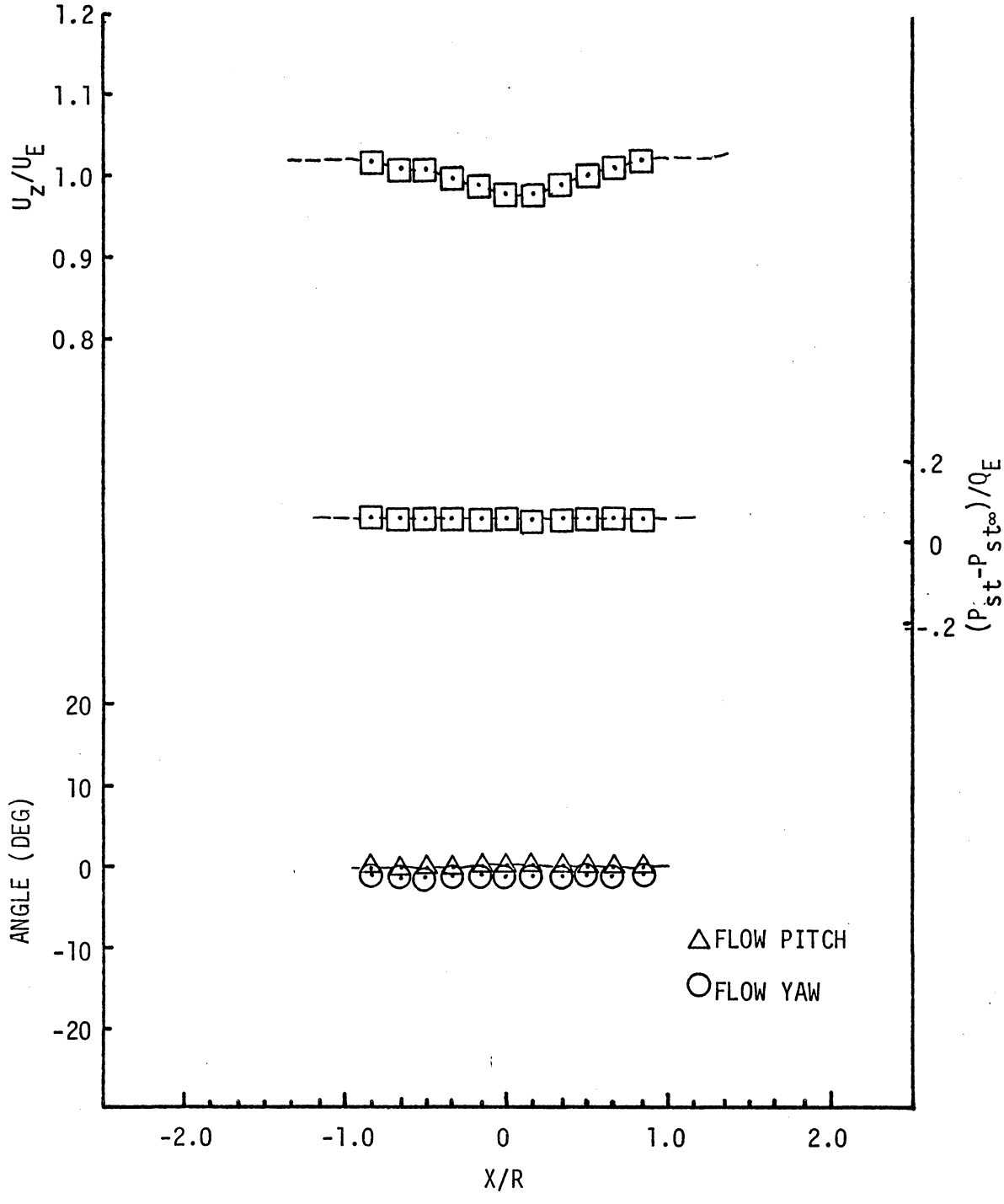

Fig. 24 MEAN AXIAL VELOCITY, FLOW ANGULARITY, AND STATIC PRESSURE ACROSS THE SAIL WAKE AT Z/D=2, Y/R=1.67, α_e=-2°

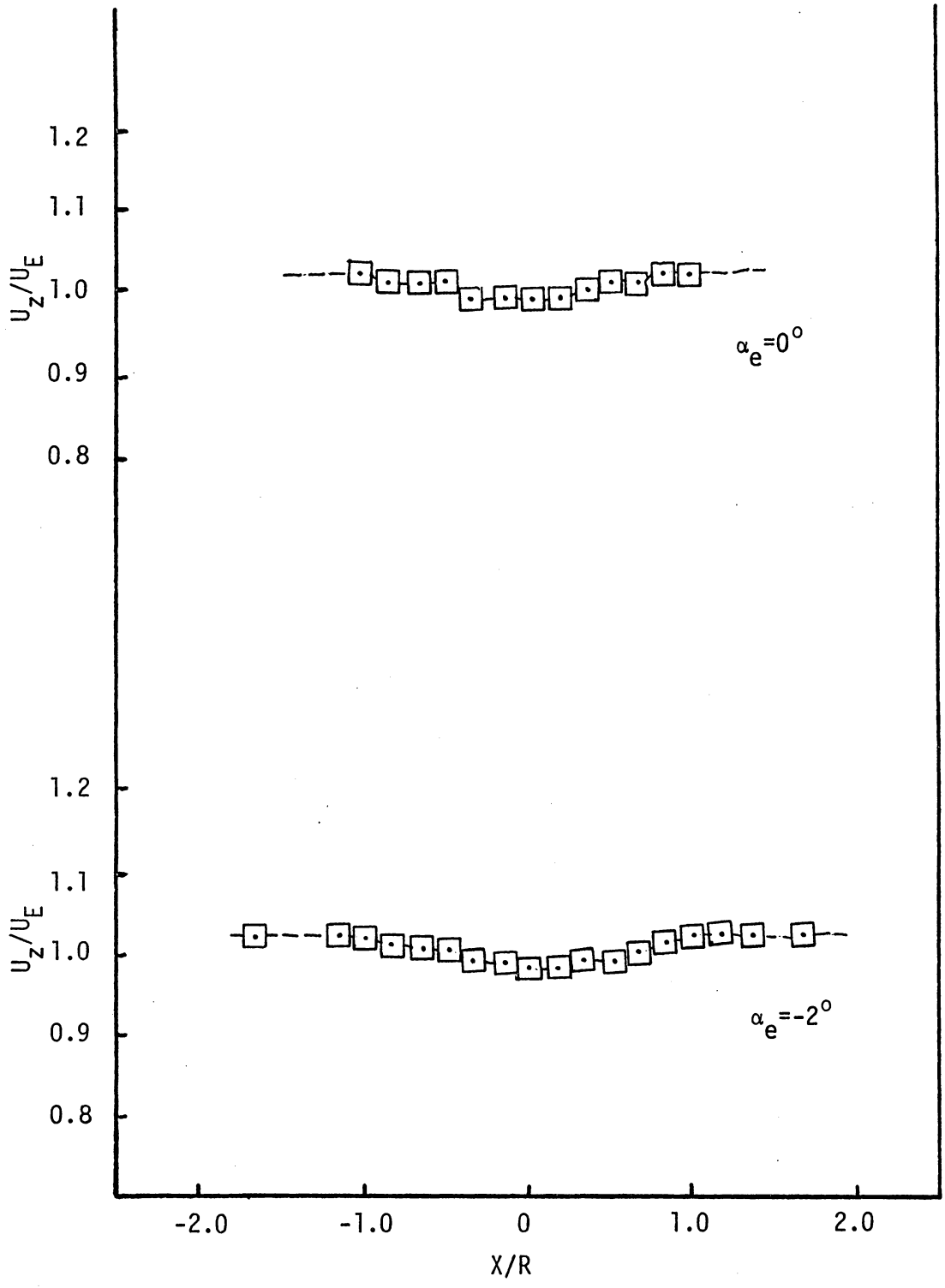

Fig. 25 MEAN AXIAL VELOCITY ACROSS THE SAIL WAKE AT Z/D=10, Y/R=1.67

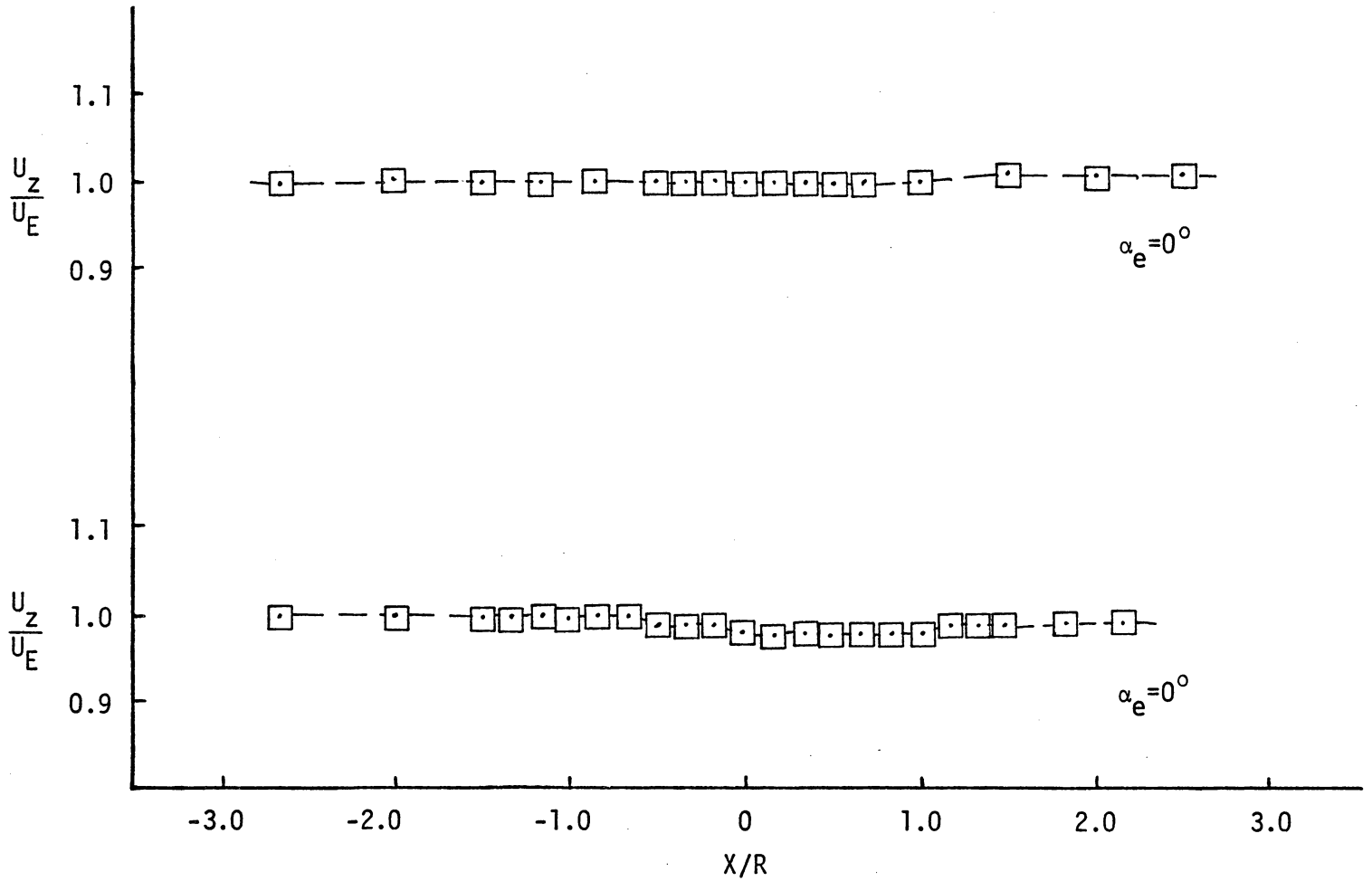

Fig. 26 MEAN AXIAL VELOCITY ACROSS SAIL WAKE AT Z/D=40, Y/R=2.33

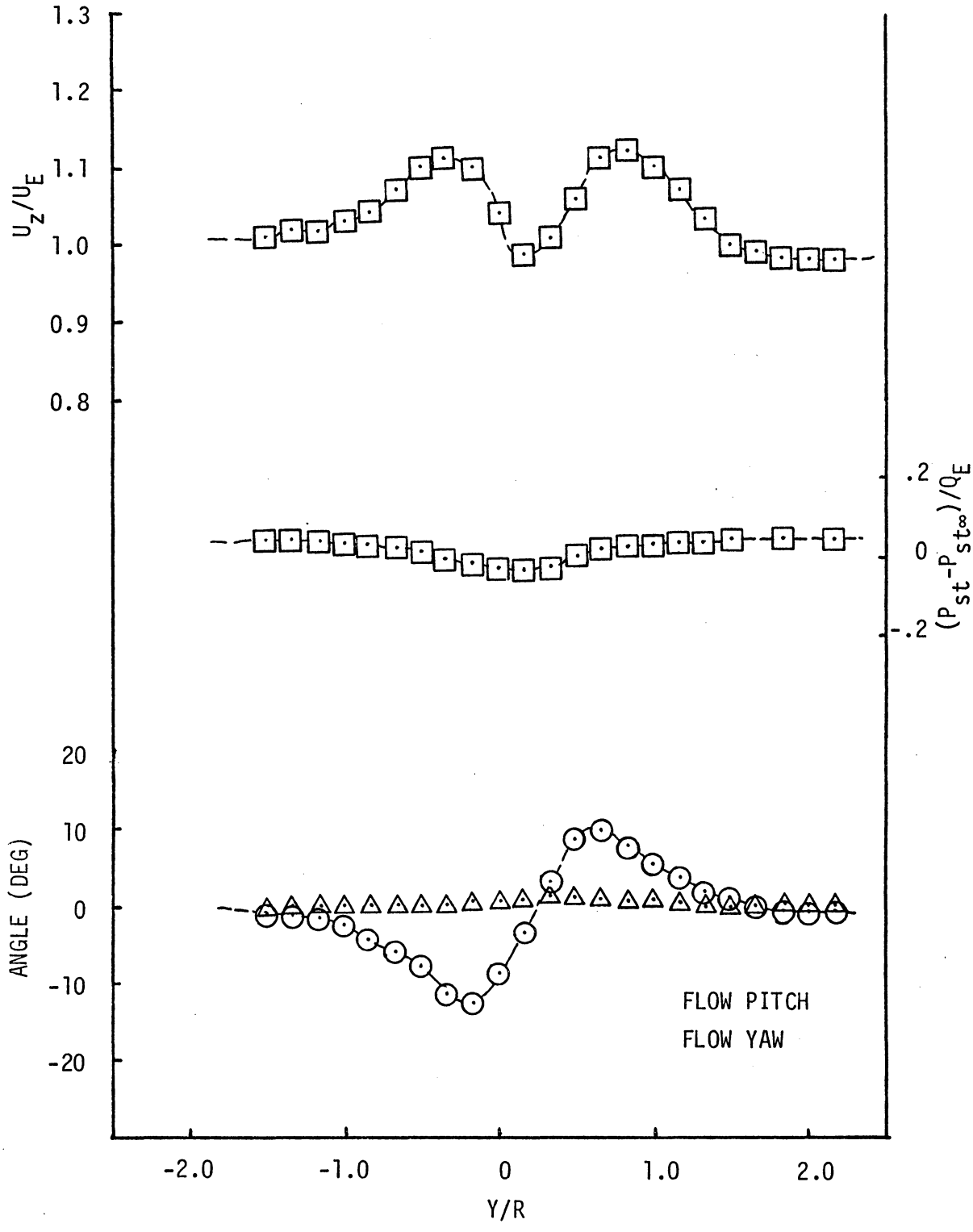

Fig. 27 MEAN AXIAL VELOCITY, FLOW ANGULARITY, AND STATIC PRESSURE VERTICAL PROFILE AT Z/D=10, X/R=0, $\alpha_e=0^\circ$

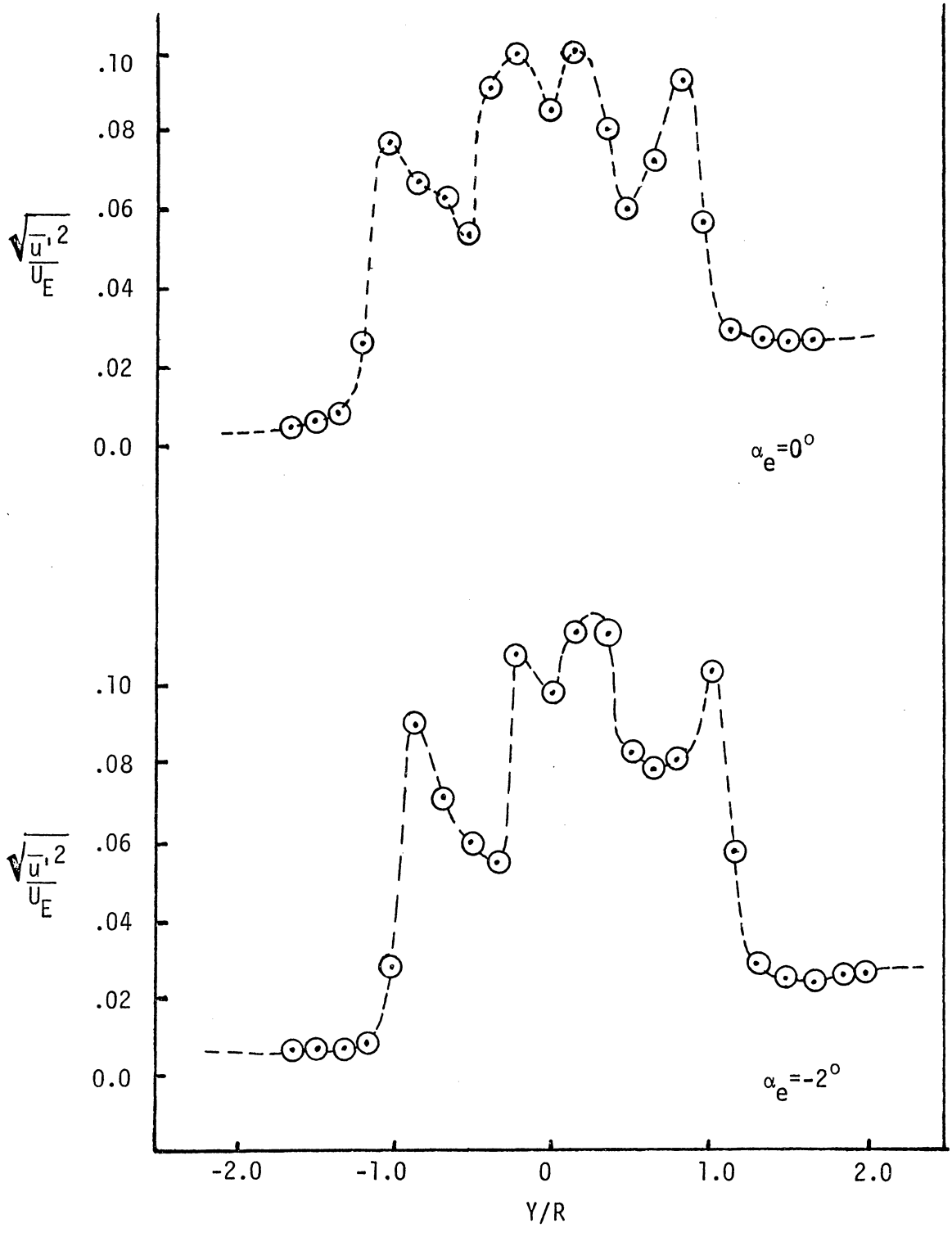

Fig.28 AXIAL TURBULENCE INTENSITY VERTICAL PROFILE AT Z/D=2, X/R=0

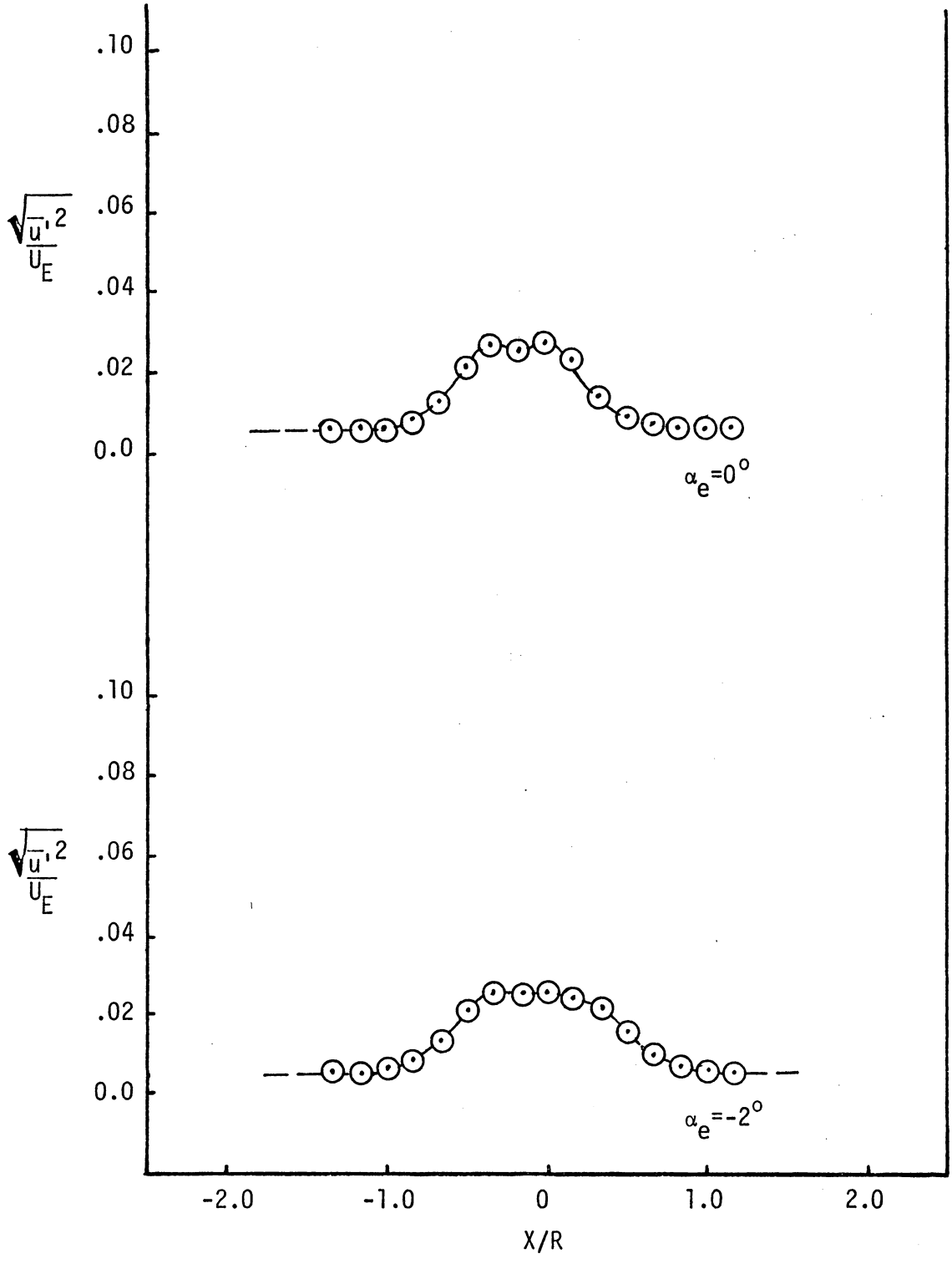

Fig. 29 AXIAL TURBULENCE INTENSITY IN SAIL WAKE AT Z/D=2, Y/R=1.67

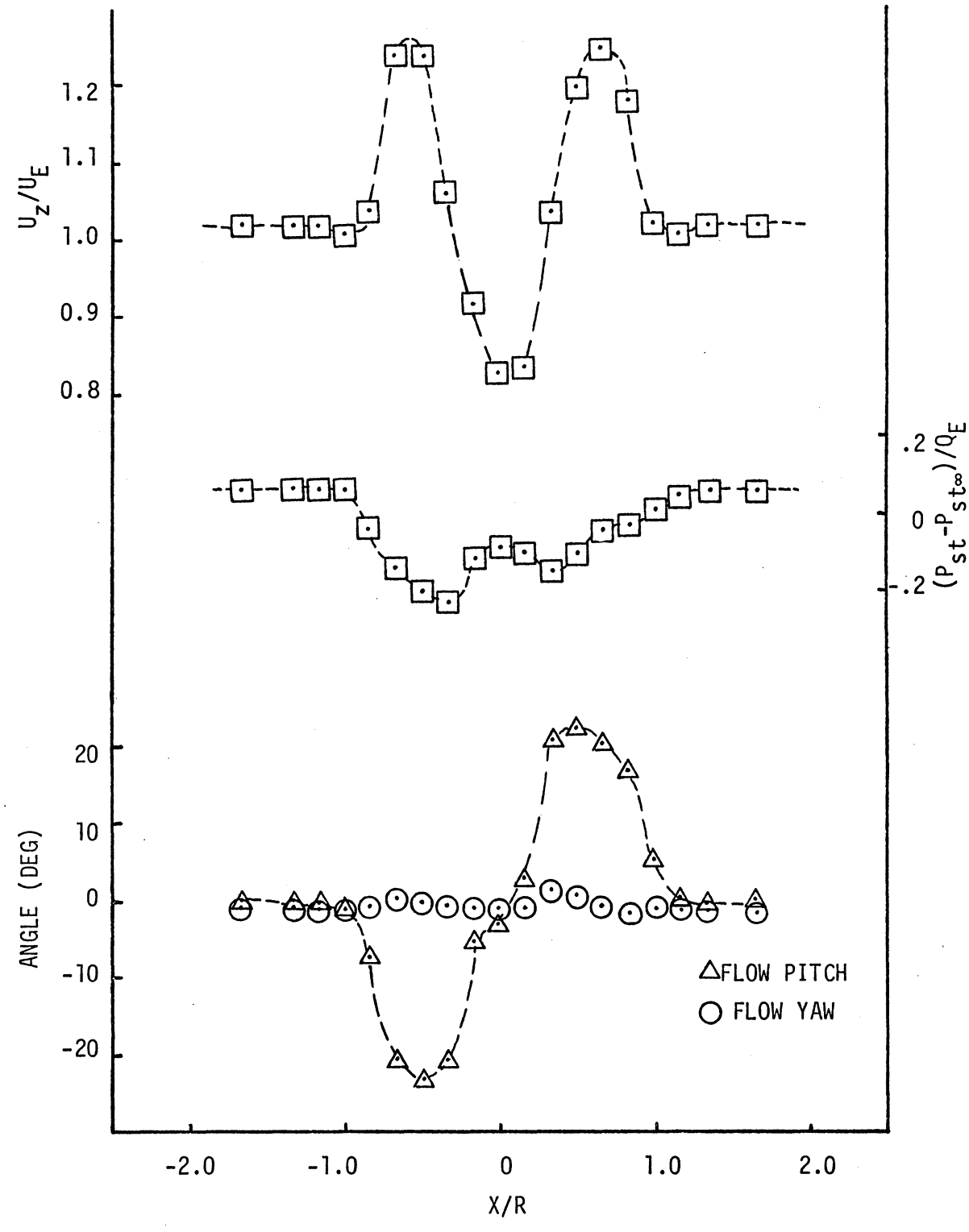

Fig. 30 MEAN AXIAL VELOCITY, FLOW ANGULARITY, AND STATIC PRESSURE HORIZONTAL PROFILE AT Z/D=2,Y/R=0, α_e=-2°

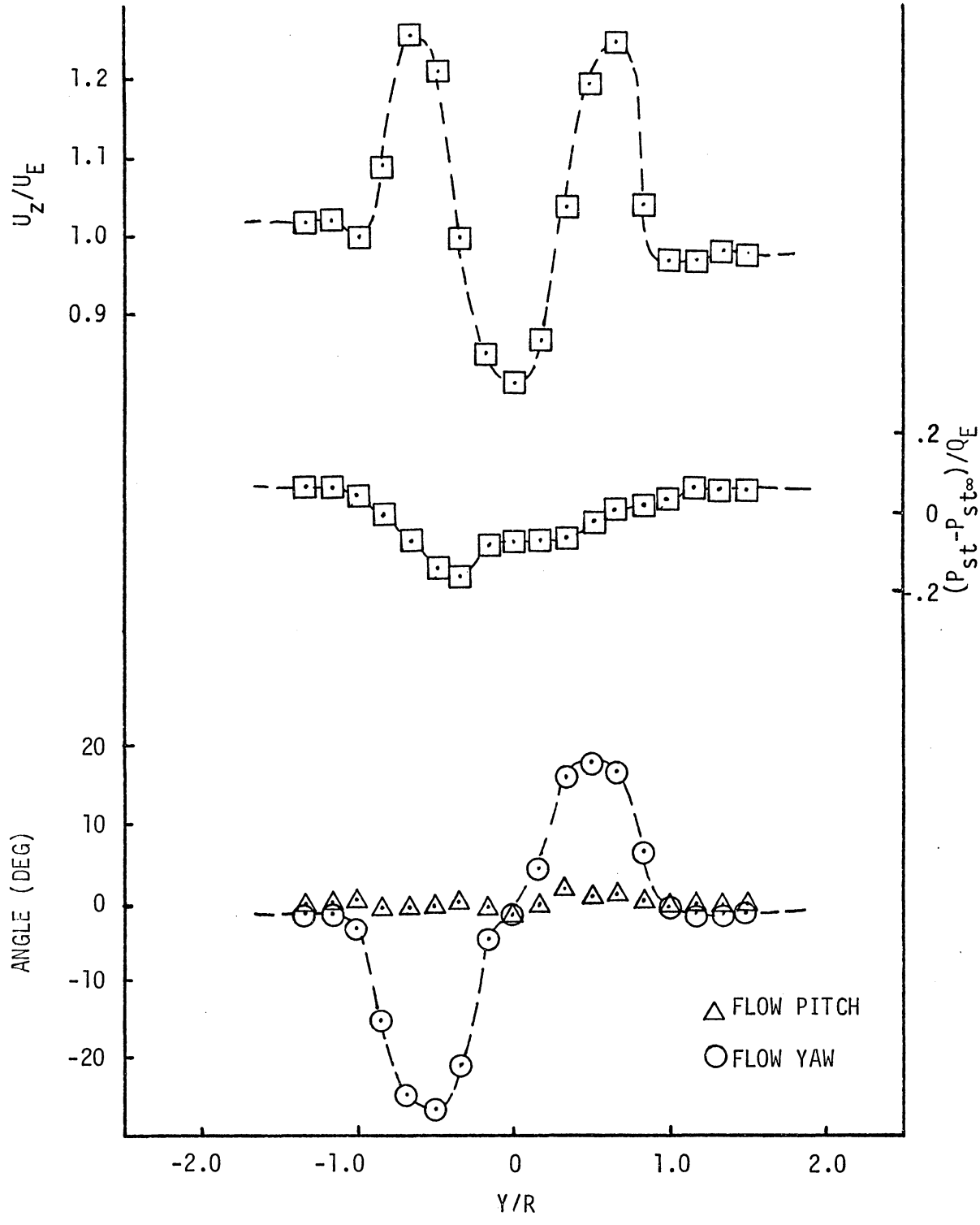

Fig. 31 MEAN AXIAL VELOCITY, FLOW ANGULARITY, AND STATIC PRESSURE VERTICAL PROFILE AT Z/D=2, X/R=0, α_e=-2°

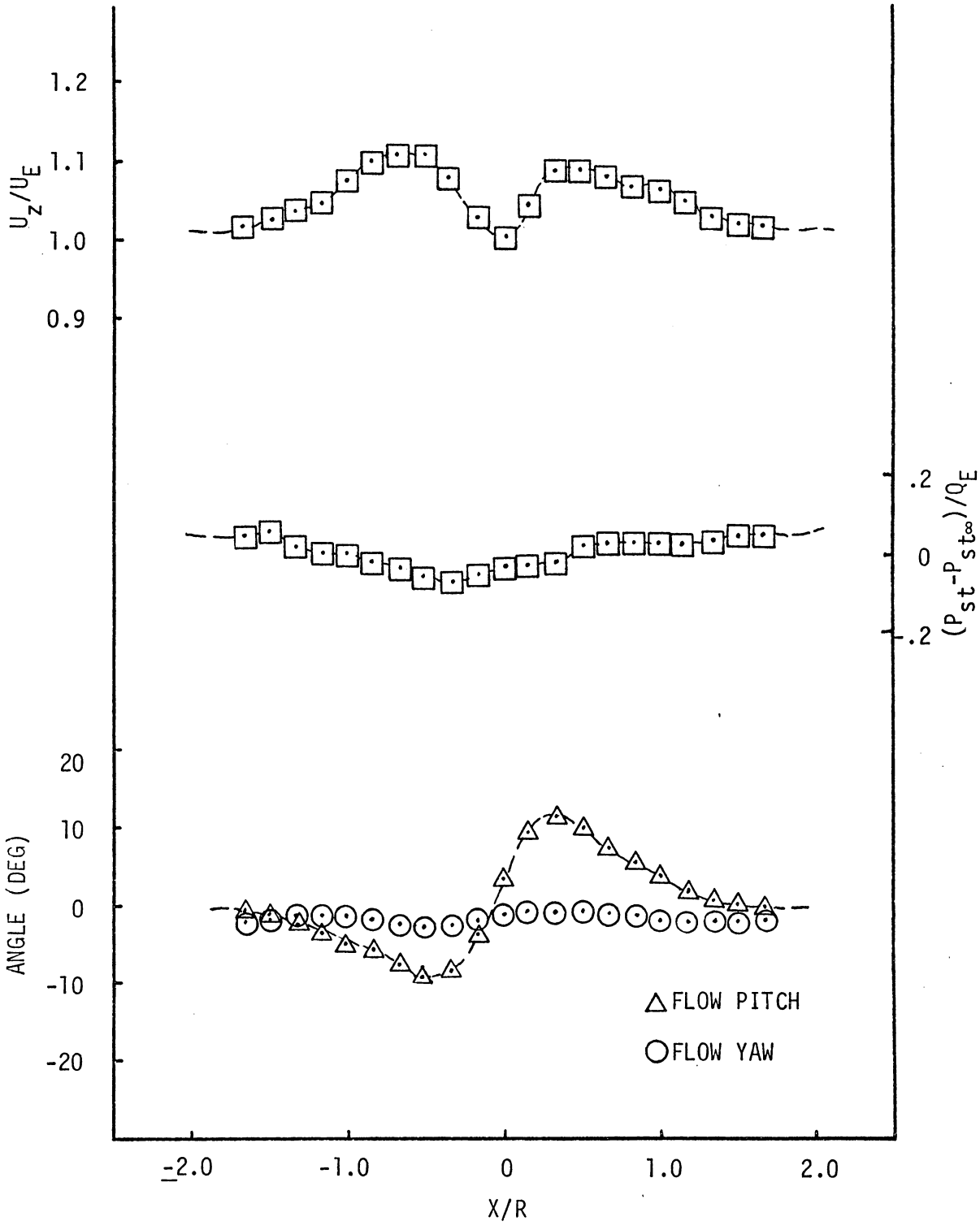

Fig. 32 MEAN AXIAL VELOCITY, FLOW ANGULARITY, AND STATIC PRESSURE HORIZONTAL PROFILE AT Z/D=10, Y/R=0, α_e=-2°

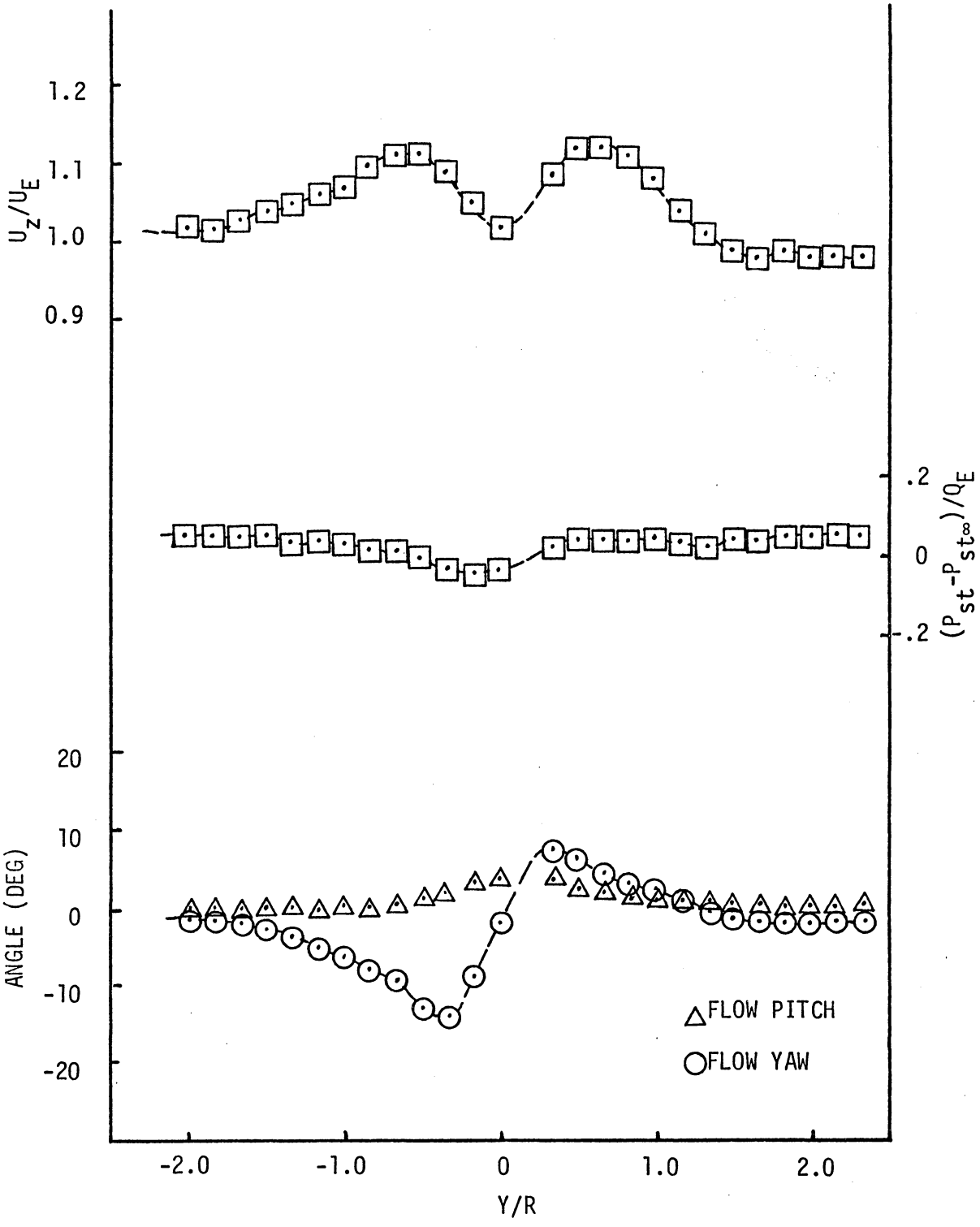

Fig. 33 MEAN AXIAL VELOCITY, FLOW ANGULARITY, AND STATIC PRESSURE VERTICAL PROFILE AT Z/D=10, X/R=0. α_e=-2°

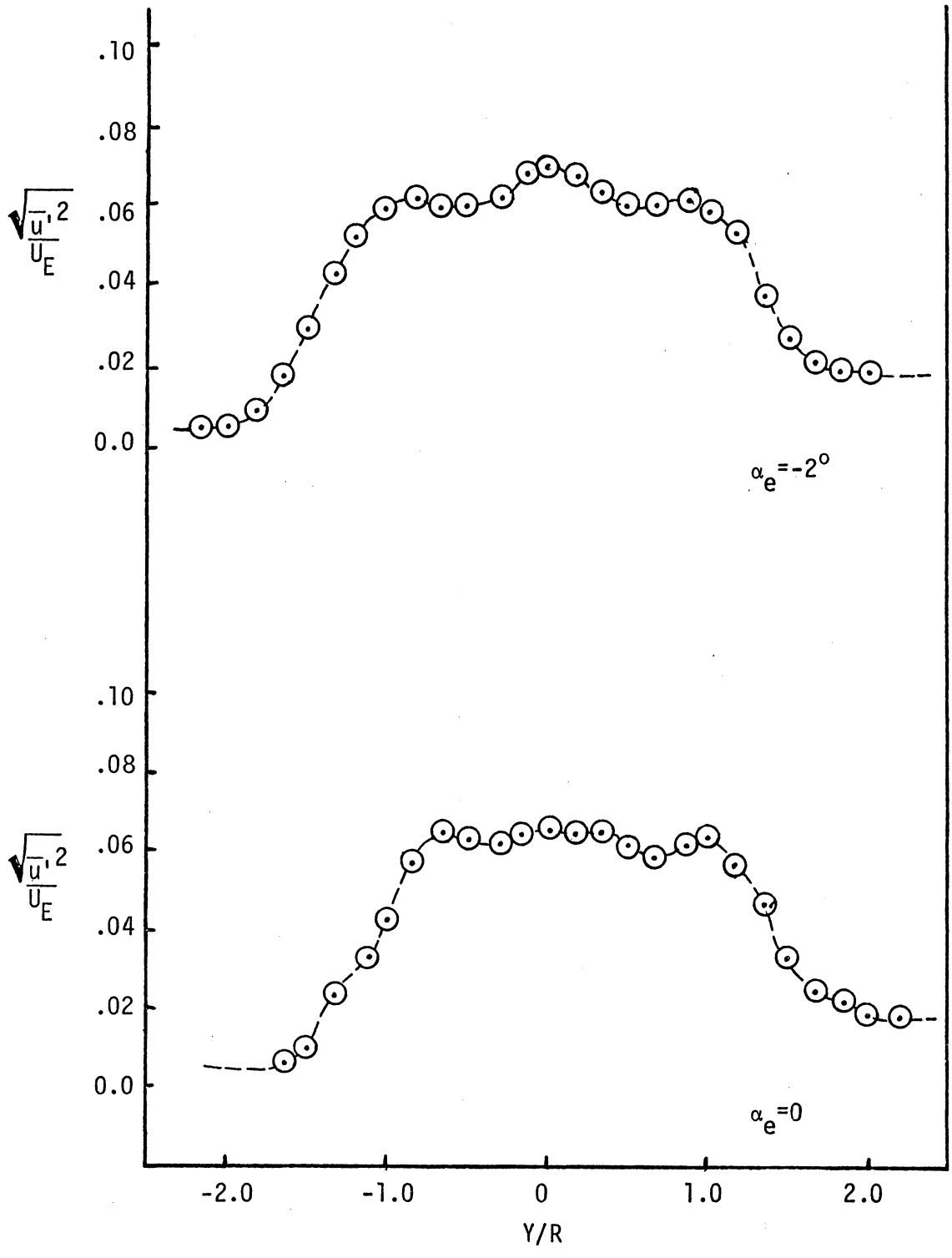

Fig. 34 AXIAL TURBULENCE INTENSITY VERTICAL PROFILE AT Z/D=10, X/R=0

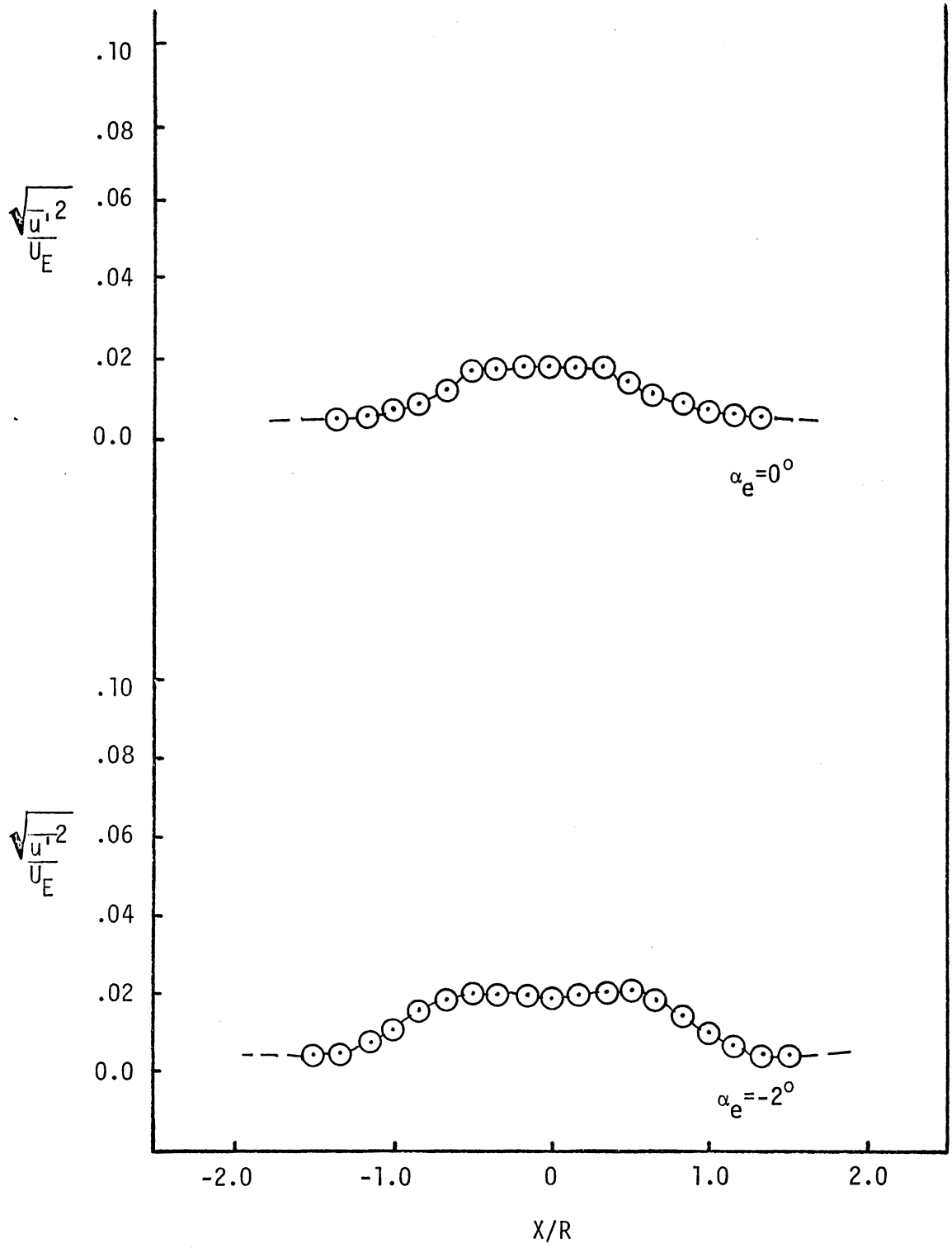

Fig. 35 AXIAL TURBULENCE INTENSITY IN SAIL WAKE AT Z/D=10, Y/R=1.67

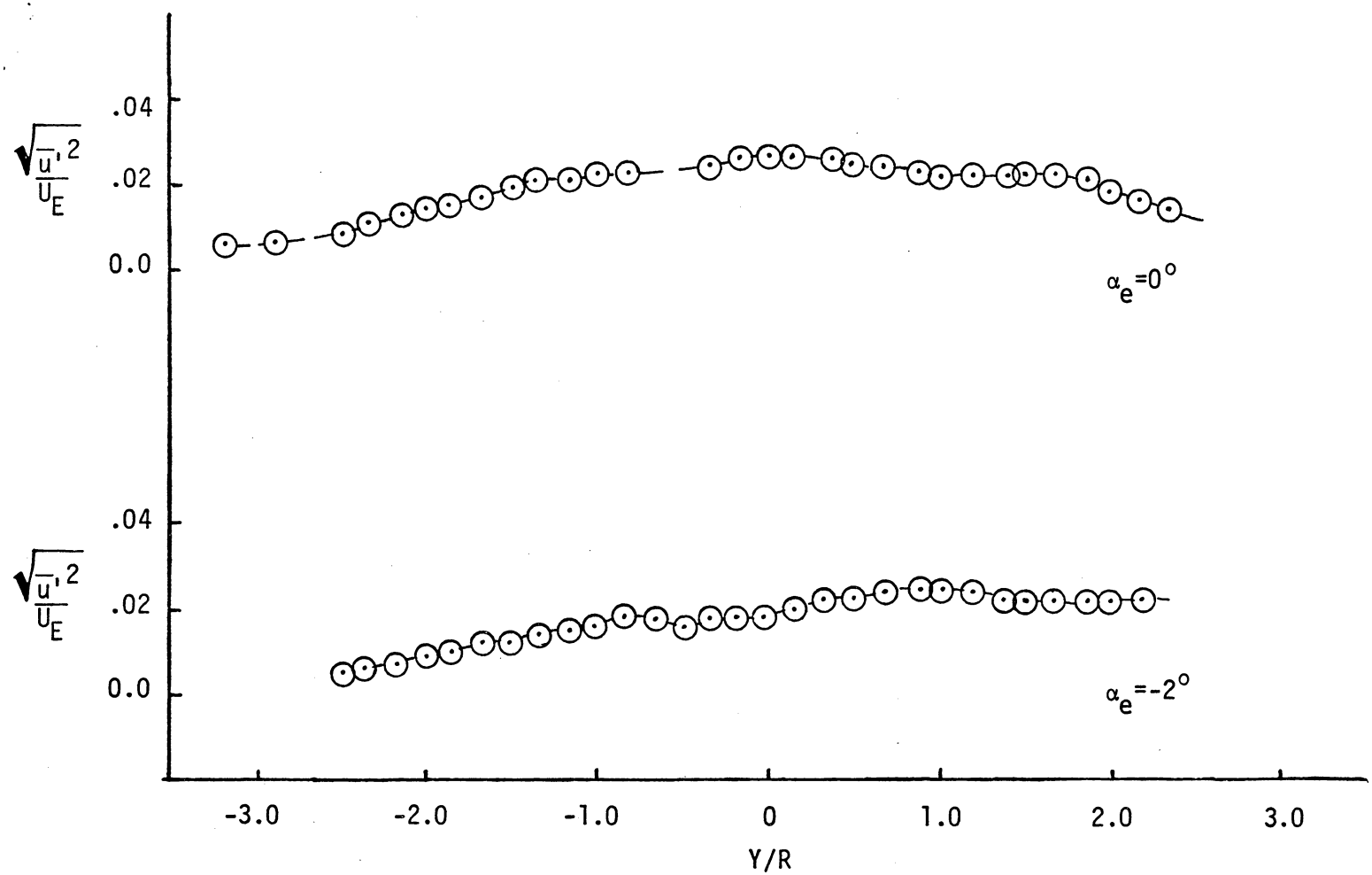

Fig. 36 AXIAL TURBULENCE INTENSITY VERTICAL PROFILE AT Z/D=40, X/R=0

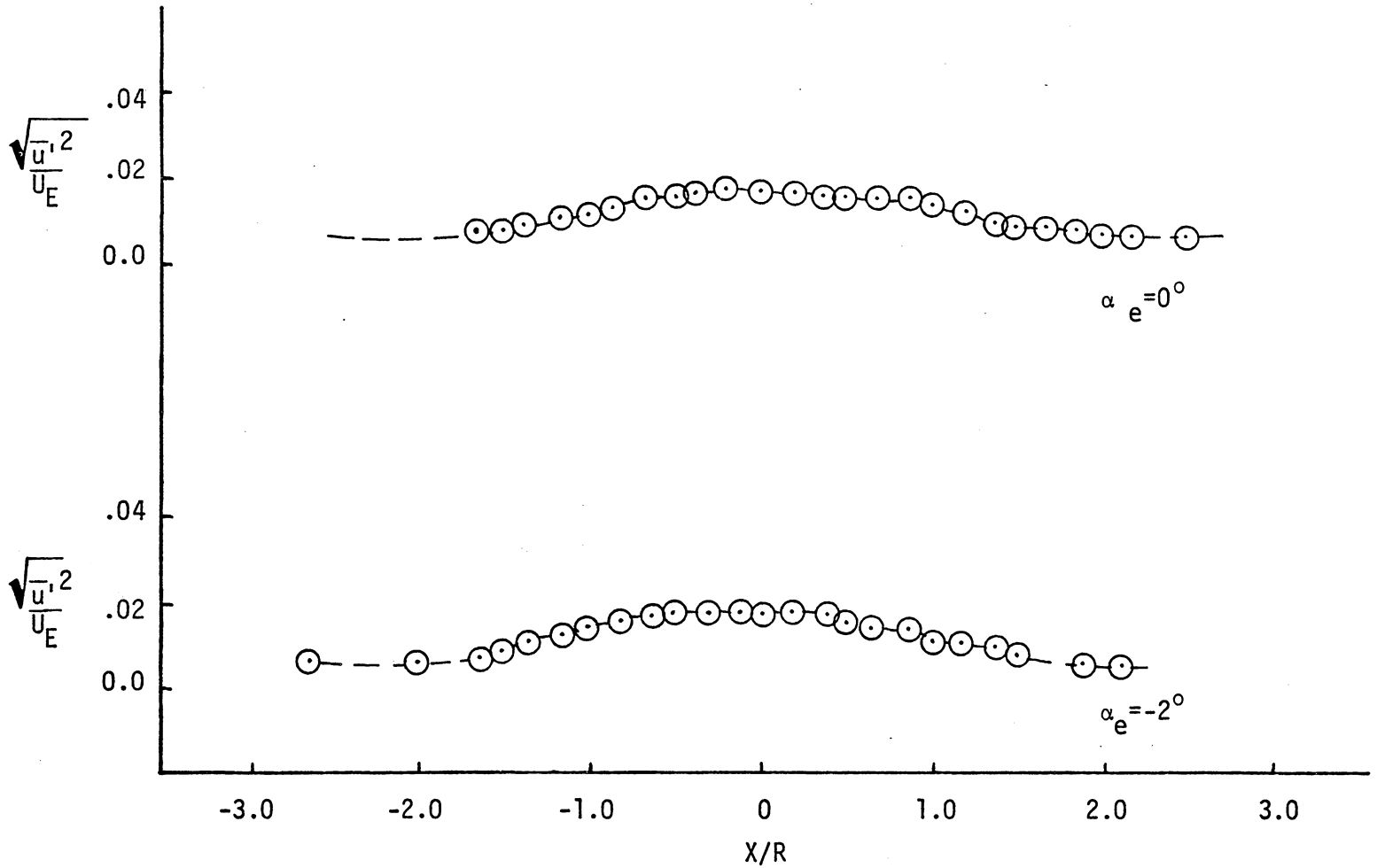

Fig. 37 AXIAL TURBULENCE INTENSITY IN SAIL WAKE AT Z/D=40, Y/R=2.33

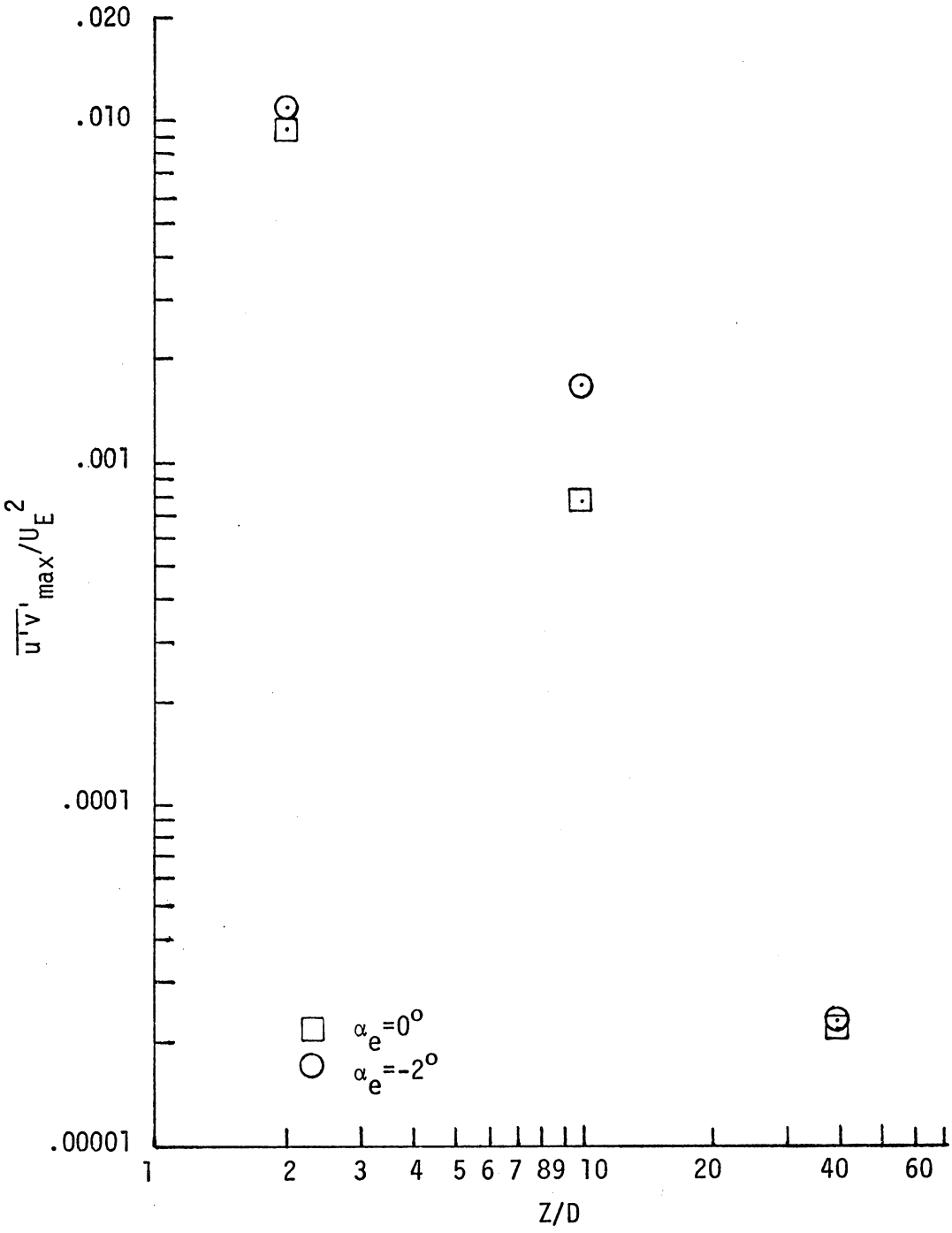

Fig. 38 MAXIMUM RADIAL SHEAR STRESS VS Z/D

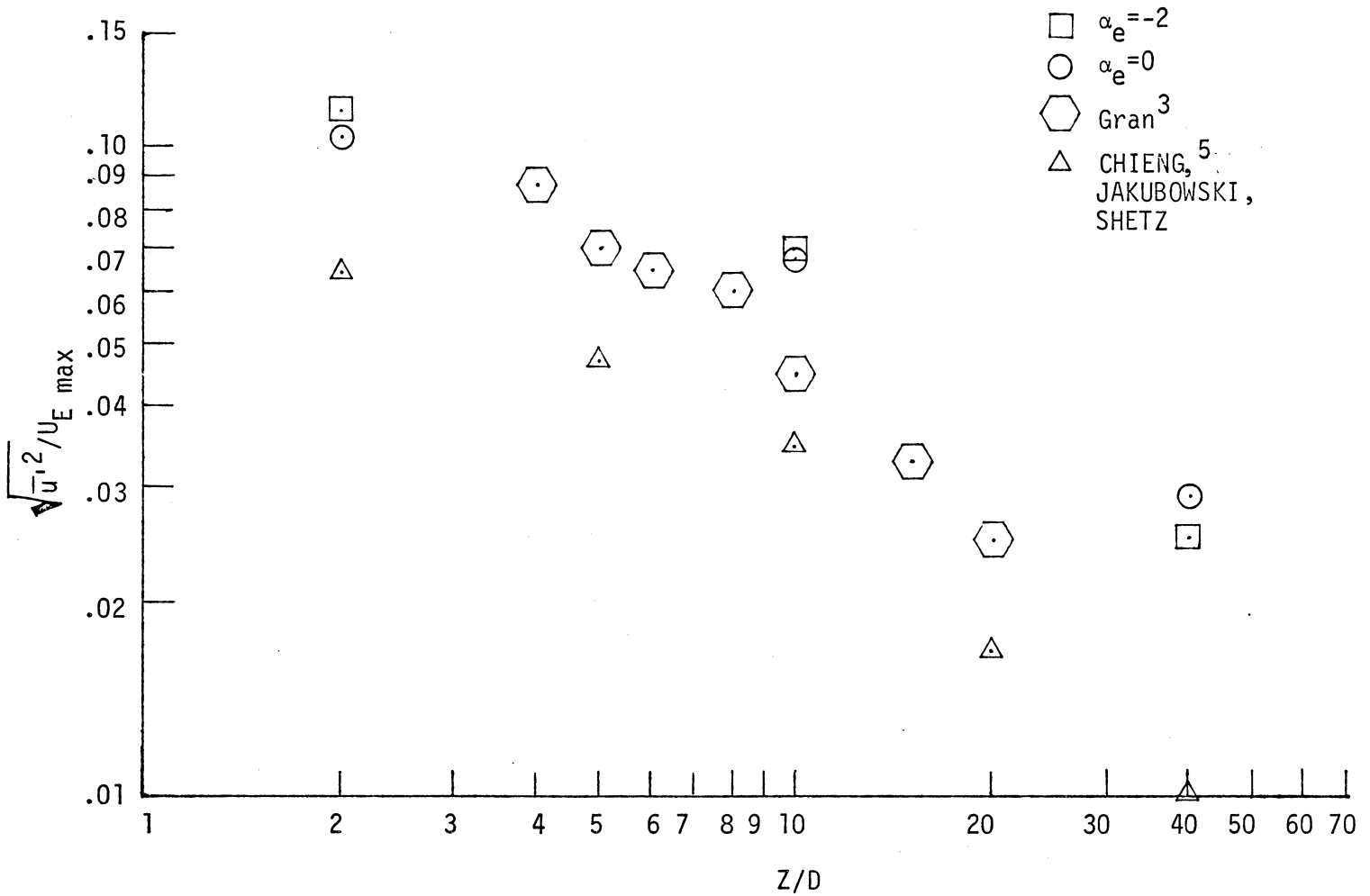

Fig. 39 MAXIMUM AXIAL TURBULENCE INTENSITY VS Z/D

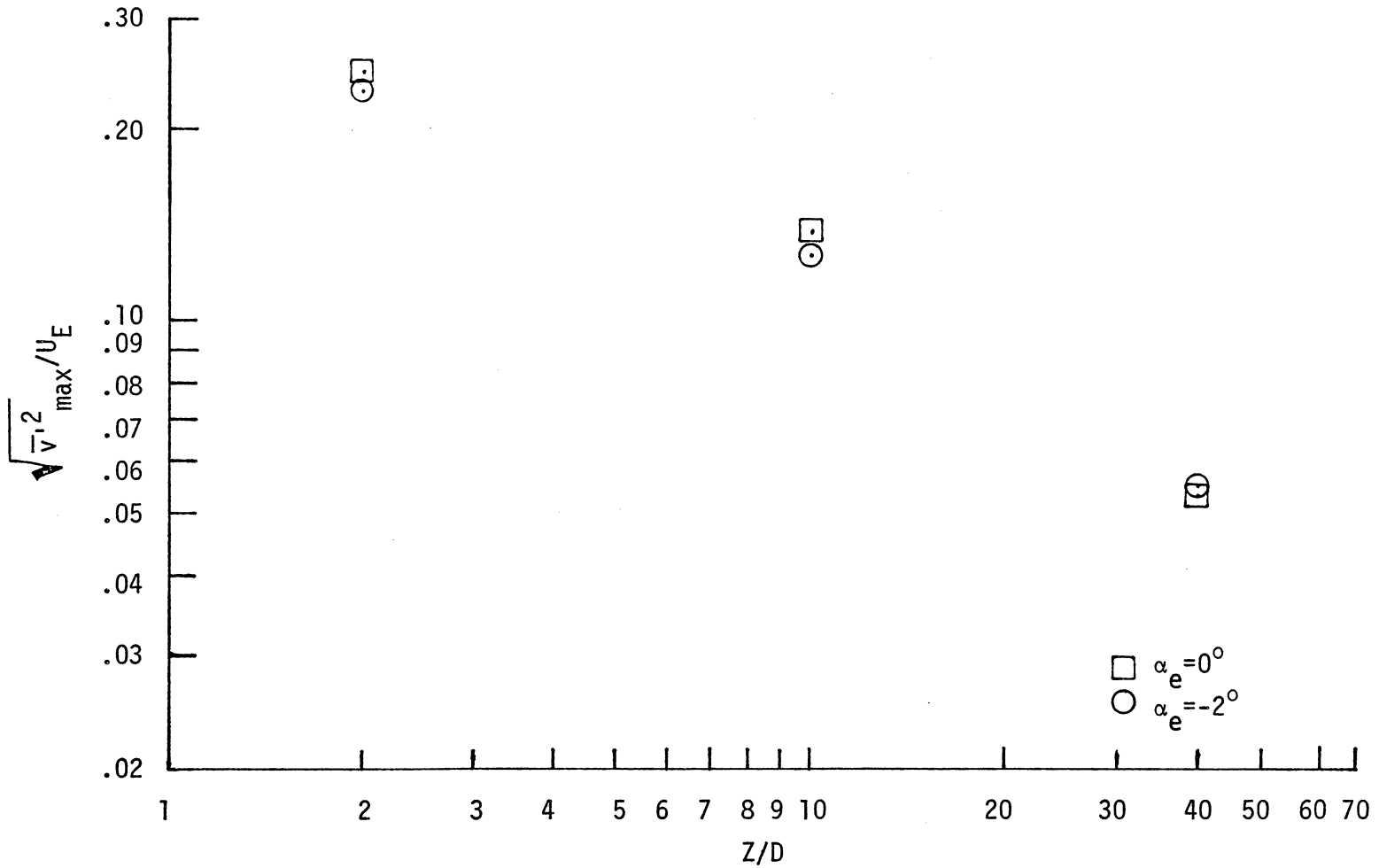

Fig. 40 MAXIMUM RADIAL TURBULENCE INTENSITY VS Z/D

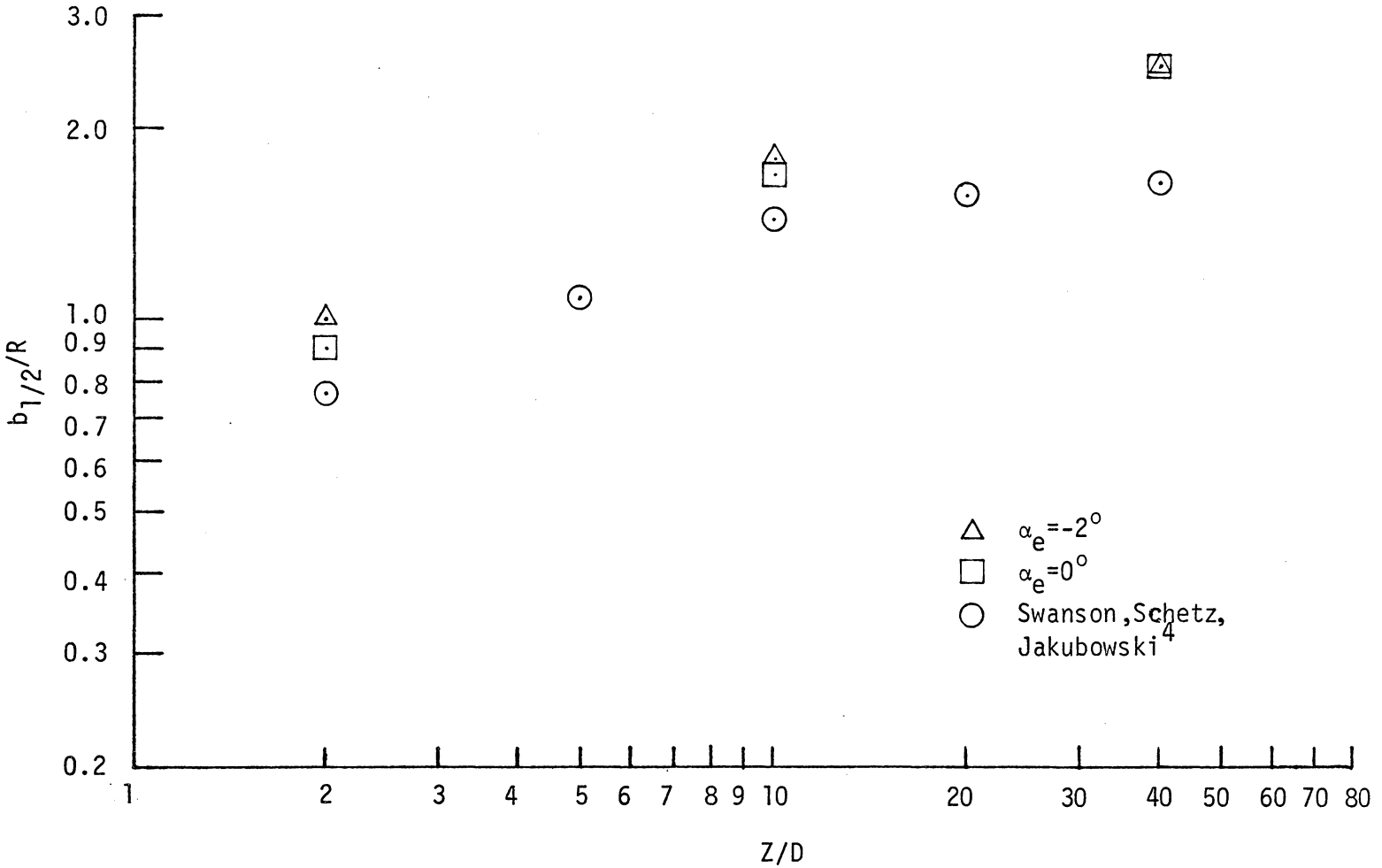

Fig. 41 HORIZONTAL WAKE GROWTH

APPENDIX A

ERROR ANALYSIS

The basic errors induced in the experiments were as follows:

1. Tunnel dynamic pressure varied slightly during testing, giving a maximum deviation of $\pm$ 1%.

2. Probe position error using the traversing mount is estimated as $\pm$ .016 inches in both vertical and horizontal directions.

3. The dynamic pressure in the wind tunnel test section was found to vary over the length of the test section by 2% of the total dynamic pressure.

4. The method of Winternitz[3] to determine static pressure was derived for flow angularity in one direction only. In the near wake region non-zero angles were measured in both the yaw and pitch directions. However, Mason and Marchman[7] found that for angularity less than $\pm$ 5° in the pitch direction the static pressure for large yaw angularity could be accurately obtained. It was, therefore, felt that adequate accuracy was obtained using the Winternitz method. Winternitz predicted accuracies of $\pm$ 1% for this method.

5. The effect of turbulence on pitot measurements is still very debatable. Goldstein in Ref. 8 asserts that the following relation should be used for the total pressure:

$$P_o = P_{st} + \frac{1}{2}\rho[\overline{(\overline{U} + u')^2} + \overline{v'^2} + \overline{w'^2}]$$

However, Hinze[8] has shown this to be inaccurate for a finite diameter pitot-tube. Therefore, because of this contraversy and the size of the turbulent quantities, no correction was made to the equation:

$$P_o = P_{st} + \frac{1}{2}\rho\overline{U}^2$$

6. The major effect on the hot wire measurements was the temperature variation. To reduce the error induced by temperature fluctuation the data was only taken after the tunnel had reached a nearly equilibrium temperature. This gave repeatable turbulence data throughout the testing. The RMS meter used is rated with an accuracy of 0.5% of the full scale deflection.

7. The self-propelled configuration was obtained very accurately by using an internally mounted strain gage balance. The self-propulsion of the model was dependent on a constant RPM of the propeller. For the wake testing the RPM was maintained at a constant level to within $\pm$ 0.2%.

8. The forward placement of the model in the wind tunnel produced a net pressure force on the model which increased the drag force. Therefore the force data presented was taken with the model further back in the test section.

9. Due to large flow angularity, the cross-wire measurements are adversly effected. The quantitative effect of this is still not known and therefore the radial turbulence intensity and shear stress results should be interpreted with this in mind.

APPENDIX B

TABULATED DATA

TABLE B-1

Profiles for Q = 5.0 in H_2O, Z/D = 2, $\alpha_e = 0°$

X/R	Y/R	Flow Pitch (DEG)	Flow Yaw (DEG)	U_z/U_E	$*\sqrt{\overline{v'^2}}/U_E$	$(x10^2)$ $*\overline{u'v'}/U_E^2$	V_{Total} (fps)	$P_{st}-P_{st\infty}$ (psf)	$\sqrt{\overline{u'^2}}/U_E$
1.33	0.0	.44	-.86	1.03	.012	.0000051	146.0	1.77	.006
1.00	0.0	.64	-.96	1.03	.091	.018	146.2	1.72	.027
.83	0.0	3.7	-.86	1.02	.147	.077	146.3	1.05	.074
.67	0.0	19.7	.04	1.18	.122	.034	178.1	-1.17	.073
.50	0.0	23.2	1.4	1.28	.091	.0092	198.1	-1.97	.062
.33	0.0	23.4	2.8	1.20	.142	.078	186.2	-3.35	.053
.17	0.0	16.6	3.5	1.00	.195	.229	148.7	-4.03	.090
0.0	0.0	2.4	.74	.89	.128	.069	126.5	-2.37	.086
-.17	0.0	-1.4	.39	.90	.148	.129	128.8	-2.35	
-.33	0.0	-6.4	1.5	.95	.189	.363	135.9	-3.21	.087
-.50	0.0	-23.4	2.0	1.13	.151	.948	175.8	-5.75	.097
-.67	0.0	-23.6	1.6	1.27	.105	.032	197.5	-4.80	.061
-.83	0.0	-19.9	1.4	1.20	.203	.222	182.9	-3.12	.063
-1.0	0.0	-4.0	-.86	1.03	.116	.036	147.5	.1738	.088
-1.17	0.0	0.0	-.86	1.03	.043	.00054	146.7	1.75	.055
-1.33	0.0	.25	-.86	1.03	.015	.000007	146.9	1.99	.017
-.83	1.67	.25	-.86	1.02	.010	.000003	146.1	1.95	.008
-.67	1.67	.25	-.86	1.02	.015	.000009	146.1	1.95	.013
-.50	1.67	.25	-.86	1.02	.023	.000072	145.5	1.93	.022
-.33	1.67	.39	-.96	1.00	.035	.00042	142.6	2.01	.027
-.17	1.67	.25	-.86	.98	.043	.00079	140.5	2.12	.026
0.0	1.67	.34	-.86	.98	.042	.00081	140.6	2.13	.027
.17	1.67	.30	-.91	1.00	.043	.00065	143.0	2.18	.023
.33	1.67	.25	-.86	1.02			145.9	2.17	.014
.50	1.67	.34	-.86	1.02	.023	.000059	146.3	2.18	.009

TABLE B-1 (Continued)

X/R	Y/R	Flow Pitch (DEG)	Flow Yaw (DEG)	U_z/U_E	$*\sqrt{\overline{v'^2}}/U_E$	$(x10^2)$ $*\overline{u'v'}/U_E^2$	V_{Total} (fps)	$P_{st}-P_{st\infty}$ (psf)	$\sqrt{\overline{u'^2}}/U_E$
0.0	2.0	.49	-.91	1.00			142.0	2.0	.027
0.0	1.83	.44	-.91	1.00			142.0	1.95	.027
0.0	1.67	.54	-.91	.99			140.6	1.94	.027
0.0	1.50	.49	-.91	.99	.043	.00070	140.5	1.98	.027
0.0	1.33	.49	-.91	.99	.046	.00085	140.8	1.99	.027
0.0	1.17	.49	-.86	.99	.068	.0027	140.8	2.01	.030
0.0	1.00	.64	-.61	1.00	.149	.0511	142.2	1.35	.058
0.0	.83	1.63	2.6	1.02	.247	.330	146.0	1.20	.093
0.0	.67	4.4	14.9	1.20	.130	.046	178.5	.76	.073
0.0	.50	4.9	19.0	1.27	.143	.028	192.4	.03	.060
0.0	.33	6.3	18.7	1.18	.183	.133	179.7	-1.06	.080
0.0	.17	5.9	10.0	.97	.205	.203	141.6	-1.74	
0.0	0.0	2.4	.54	.88	.158	.080	125.7	-2.39	.085
0.0	-.17	2.2	-2.9	.88	.208	.271	125.9	-2.08	.100
0.0	-.33	5.1	-14.7	.97			144.7	-4.39	.091
0.0	-.50	4.4	-26.5	1.19			191.0	-5.6	.054
0.0	-.67	2.5	-25.4	1.28	.128	.060	203.0	-2.6	.063
0.0	-.83	1.4	-20.5	1.17	.226	.195	178.5	-0.75	.068
0.0	-1.0	1.0	-4.1	1.02	.143	.053	146.6	1.22	.077
0.0	-1.17	.30	-.86	1.03	.054	.00093	147.2	1.75	.027
0.0	-1.33	.30	-.86	1.03	.017	.000010	147.4	1.76	.009

* Measurements taken in high flow angularity

TABLE B-2

Profiles for Q = 5.0 in H_2O, Z/D = 2, α_e = -2°

X/R	Y/R	Flow Pitch (DEG)	Flow Yaw (DEG)	U_z/U_E	$*\sqrt{\overline{v'^2}}/U_E$	$(x10^2)$ $*\overline{u'v'}/U_E^2$	V_{Total} (fps)	$P_{st}-P_{st\infty}$ (psf)	$\sqrt{\overline{u'^2}}/U_E$
1.67	0.0	.10	-.96	1.02	.0081	.000002	148.1	1.50	.006
1.33	0.0	-.25	-1.0	1.02	.018	.000066	148.3	1.52	.007
1.17	0.0	.20	-1.1	1.01	.058	.0064	147.4	1.34	.016
1.00	0.0	5.4	-1.0	1.02	.138	.143	149.7	.39	.048
.83	0.0	17.1	-1.2	1.18	.197	.574	179.5	-.93	.092
.67	0.0	20.5	-.26	1.25	.141	.160	193.6	-1.06	.088
.50	0.0	22.5	.99	1.20	.081	.019	189.7	-2.55	.069
.33	0.0	21.1	1.7	1.04	.096	.043	162.3	-3.76	.050
.17	0.0	3.2	-.56	.84	.223	1.01	122.3	-2.61	.067
0.0	0.0	-2.2	-1.0	.83	.176	.463	121.9	-2.33	.098
-.17	0.0	-4.7	-.71	.92	.188	.664	134.6	-2.96	.083
-.33	0.0	-20.5	-.21	1.06	.203	1.09	165.4	-6.01	.091
-.50	0.0	-23.3	.09	1.24	.203	1.10	196.7	-5.30	.113
-.67	0.0	-20.5	.64	1.24	.108	.094	193.3	-3.66	.062
-.83	0.0	-7.0	-.76	1.04	.189	.474	153.4	-1.10	.063
-1.00	0.0	-1.0	-1.2	1.01	.154	.357	145.9	1.52	.088
-1.17	0.0	-.44	-1.1	1.02	.050	.0039	147.0	1.62	.059
-1.33	0.0	-.34	-.86	1.02	.015	.000024	146.9	1.71	.020
-1.67	0.0	-.34	-.86	1.02	.0081	.000002	146.9	1.71	.006
-.83	1.67	-.15	-.91	1.02	S	S	147.0	1.69	.009
-.67	1.67	0.0	-1.06	1.01	S	S	146.4	1.64	.014
-.50	1.67	.10	-.96	1.01	S	S	146.0	1.62	.021
-.33	1.67	.25	-1.1	1.00	S	S	144.4	1.59	.025
-.17	1.67	.30	-1.1	.99	S	S	142.4	1.56	.025
0.0	1.67	.39	-1.0	.98	.040	.00080	141.8	1.59	.026

TABLE B-2 (Continued)

X/R	Y/R	Flow Pitch (DEG)	Flow Yaw (DEG)	U_z/U_E	$*\sqrt{\overline{v'^2}}/U_E$	$(x10^2)$ $*\overline{u'v'}/U_E^2$	V_{Total} (fps)	$P_{st}-P_{st\infty}$ (psf)	$\sqrt{\overline{u'^2}}/U_E$
.17	1.67	.39	-.91	.98	.041	.00070	142.1	1.55	.025
.33	1.67	.39	-.86	.99	.035	.00021	143.8	1.59	.021
.50	1.67	.25	-.91	1.00	.023	.00006	145.3	1.53	.016
.67	1.67	.20	-.96	1.01			146.3	1.54	.011
.83	1.67	.15	-1.1	1.02			147.1	1.56	.008
0.0	1.50	.25	-.96	.98	.041	.0027	141.7	1.56	.026
0.0	1.33	.25	-.76	.98	.049	.0078	140.5	1.54	.030
0.0	1.17	.15	-.66	.97	.097	.041	139.4	1.54	.051
0.0	1.00	.15	-.11	.97	.230	1.09	139.4	0.85	.103
0.0	.83	.74	6.4	1.04	.215	.688	151.0	0.56	.081
0.0	.67	1.5	16.7	1.25	.162	.215	188.8	0.22	.078
0.0	.50	1.3	18.1	1.20	.174	.361	182.1	-.94	.083
0.0	.33	2.5	16.5	1.04	.220	1.10	157.0	-1.88	.113
0.0	.17	.20	4.9	.87	.178	.471	125.7	-1.94	.113
0.0	0.0	-1.0	-1.1	.82	.176	.456	118.1	-1.99	.098
0.0	-.17	-.54	-4.4	.85	.203	1.01	123.6	-2.22	.109
0.0	-.33	.30	-21.2	1.00	.139	.262	155.3	-4.18	.056
0.0	-.50	-.05	-26.8	1.21	.081	.0375	196.7	-3.69	.060
0.0	-.67	-.25	-24.7	1.26	.160	.348	200.5	-1.97	.071
0.0	-.83	-.34	-14.9	1.09	.212	.762	162.8	-.23	.090
0.0	-1.00	.54	-3.0	1.00	.085	.0285	145.2	1.18	.029
0.0	-1.17	.49	-1.1	1.02	.025	.00016	147.4	1.61	.008
0.0	-1.33	.30	-.96	1.02	.011	.000006	147.7	1.67	.008

* Measurements taken in high flow angularity

S Symmetric profiles

TABLE B-3

Profiles for Q = 5.0 in H_2O, Z/D = 10, $\alpha_e = 0°$

X/R	Y/R	Flow Pitch (DEG)	Flow Yaw (DEG)	U_z/U_E	$*\sqrt{\overline{v'^2}}/U_E$	$(x10^2)$ $*\overline{u'v'}/U_E^2$	V_{Total} (fps)	$P_{st}-P_{st\infty}$ (psf)	$\sqrt{\overline{u'^2}}/U_E$
0.0	0.0	.94	-8.8	1.04	.131	.0781	151.7	-.90	.065
0.0	.17	1.2	-3.1	.99	.135	.0624	144.4	-.91	.066
0.0	.33	1.6	3.2	1.01	.138	.0645	147.0	-.77	.064
0.0	.50	1.4	8.5	1.06	.128	.0485	156.0	-.14	.061
0.0	.67	1.3	9.6	1.11	.122	.0462	162.9	.41	.058
0.0	.83	1.0	7.8	1.12	.126	.0633	165.3	.63	.061
0.0	1.00	.94	5.6	1.10	.128	.0760	161.5	.76	.063
0.0	1.17	.59	3.9	1.07	.118	.0583	156.7	.82	.058
0.0	1.33	.34	2.1	1.03	.101	.0309	151.6	.92	.046
0.0	1.50	.30	.54	1.00	.076	.0099	147.2	1.02	.034
0.0	1.67	.25	-.01	.99	.0173	.000037	141.8	.58	.025
0.0	1.83	.25	-.61	.98			141.0	1.09	.022
0.0	2.00	.25	-.66	.98	.030	.00030	141.0	1.06	.019
0.0	2.17	.25	-.76	.98			141.0	1.11	.018
0.0	-.17	.89	-12.6	1.10	.120	.0584	161.7	-.58	.065
0.0	-.33	.44	-11.1	1.11	.116	.0231	163.6	-.21	.061
0.0	-.50	.25	-7.6	1.10			160.2	.29	.063
0.0	-.67	.25	-5.9	1.07	.107	.0289	155.0	.53	.064
0.0	-.83	.30	-4.3	1.04	.091	.0143	150.9	.77	.057
0.0	-1.00	.30	-2.6	1.03	.070	.0054	148.5	.92	.044
0.0	-1.17	.30	-1.5	1.02	.050	.0013	147.4	1.12	.033
0.0	-1.33	.25	-.91	1.02	.034	.00023	147.1	1.17	.020
0.0	-1.50	.15	-.81	1.01	.020	.00011	147.1	1.16	.012
-.33	0.0	-10.2	-2.4	1.08	S	S	158.8	-2.43	.062
-.17	0.0	-5.5	-3.3	1.03	S	S	150.2	-2.11	.065

TABLE B-3 (Continued)

X/R	Y/R	Flow Pitch (DEG)	Flow Yaw (DEG)	U_z/U_E	$*\sqrt{\overline{v'^2}}/U_E$	$(x10^2)$ $*\overline{u'v'}/U_E^2$	V_{Total} (fps)	$P_{st}-P_{st\infty}$ (psf)	$\sqrt{\overline{u'^2}}/U_E$
0.0	0.0	1.2	-3.7	1.00	.131	.0781	144.7	-.98	.066
.17	0.0	8.0	-3.4	1.03	.118	.0571	151.1	-.55	.065
.33	0.0	11.1	-2.8	1.08	.097	.0277	159.6	-.54	.061
.50	0.0	9.5	-2.3	1.10	.090	.0240	161.3	.23	.062
.67	0.0	7.3	-2.0	1.10	.091	.0271	161.1	.28	.064
.83	0.0	5.4	-1.8	1.09	.096	.034	158.9	.29	.065
1.00	0.0	4.0	-1.7	1.07	.099	.037	155.7	.38	.061
1.17	0.0	2.5	-1.5	1.05	.088	.020	151.8	.30	.047
1.33	0.0	.94	-1.2	1.03	.060	.0042	148.9	.84	.032
1.50	0.0	.25	-.91	1.01			146.7	.98	.018
1.67	0.0	.15	-.91	1.01	.017	.000037	146.0	.95	.006
0.0	0.0	3.0	-2.4	1.01	.131	.0781	144.8	-1.08	.067
-.33	0.0	-9.4	-1.7	1.08	S	S	156.9	-2.42	.062
-.50	0.0	-10.6	-1.3	1.11	S	S	162.6	-2.08	.059
-.67	0.0	-8.0	-.86	1.12	S	S	161.8	-1.17	.060
-.83	0.0	-6.2	-.86	1.10	S	S	159.6	-.68	.061
-1.00	0.0	-4.5	-.56	1.08	S	S	156.3	-.13	.054
-1.17	0.0	-3.0	-.56	1.07	S	S	153.2	.15	.054
-1.33	0.0	-1.5	-.61	1.05	S	S	150.8	.40	.042
-1.50	0.0	-.54	-.81	1.03	S	S	148.3	1.25	.027
-1.67	0.0	.10	-.86	1.02	S	S	146.7	1.31	.011
-1.83	0.0	.25	-.86	1.02	S	S	146.2	1.43	
-2.00	0.0	.25	-.96	1.01	S	S	145.7	1.46	
-1.00	2.00	.15	-1.1	1.02	S	S	145.8	1.35	.007
-.83	2.00	.25	-1.1	1.01	S	S	145.7	1.34	.009
-.67	2.00	.30	-1.1	1.01	S	S	144.8	1.31	.013
-.50	2.00	.34	-1.1	1.01	S	S	145.6	1.34	.017

TABLE B-3 (Continued)

X/R	Y/R	Flow Pitch (DEG)	Flow Yaw (DEG)	U_z/U_E	$*\sqrt{\overline{v'^2}}/U_E$	$(x10^2)$ $*\overline{u'v'}/U_E^2$	V_{Total} (fps)	$P_{st}-P_{st\infty}$ (psf)	$\sqrt{\overline{u'^2}}/U_E$
-.33	2.00	.44	-1.1	.99	S	S	142.7	1.24	.018
-.17	2.00	.44	-1.1	.99	S	S	142.0	1.22	.018
0.0	2.00	.44	-1.1	.99	.030	.00030	142.0	1.22	.018
.17	2.00	.44	-1.1	.99	.054	.0022	142.6	1.24	.018
.33	2.00	.44	-1.1	1.00	.049	.0014	143.9	1.28	.017
.50	2.00	.44	-1.1	1.01	.041	.00070	144.7	1.31	.015
.67	2.00	.44	-1.1	1.01	.030	.00021	145.4	1.34	.012
.83	2.00	.44	-1.1	1.02	.022	.000059	145.8	1.35	.009
1.00	2.00	.39	-1.3	1.02	.016	.000019	146.2	1.20	.007

* Measurements taken in high flow angularity

S Symmetric profiles

TABLE B-4

Profiles for Q = 5.0 in H_2O, Z/D = 10, α_e = -2°

X/R	Y/R	Flow Pitch (DEG)	Flow Yaw (DEG)	U_z/U_E	$*\sqrt{\overline{v'^2}}/U_E$	$(x10^2)$ $*\overline{u'v'}/U_E^2$	V_{Total} (fps)	$P_{st}-P_{st\infty}$ (psf)	$\sqrt{\overline{u'^2}}/U_E$
-1.67	0.0	-.44	-1.2	1.02	S	S	150.0	1.40	.016
-1.50	0.0	-.89	-1.1	1.03	S	S	150.9	1.40	.076
-1.33	0.0	-1.9	-.96	1.04	S	S	153.0	.58	.039
-1.17	0.0	-2.8	-.96	1.05	S	S	155.2	.37	.047
-1.00	0.0	-4.1	-1.0	1.08	S	S	158.9	.05	.054
-.83	0.0	-5.1	-1.6	1.10	S	S	162.4	-.23	.058
-.67	0.0	-7.0	-1.9	1.11	S	S	165.5	-.73	.060
-.50	0.0	-8.6	-2.1	1.11	S	S	165.7	-1.42	.063
-.33	0.0	-8.0	-2.2	1.08	S	S	161.1	-1.74	.066
-.17	0.0	-3.0	-1.8	1.03	S	S	152.1	-1.34	.067
0.0	0.0	3.7	-1.1	1.01	.127	.168	149.6	-.81	.069
.17	0.0	9.7	-.36	1.05	.116	.126	157.0	-.34	.071
.33	0.0	11.8	-.36	1.09	.093	.060	164.2	-.25	.066
.50	0.0	9.9	-.61	1.09	.096	.066	164.3	.54	.063
.67	0.0	7.7	-.86	1.08	.104	.088	161.2	.77	.063
.83	0.0	5.9	-1.2	1.07	.108	.094	159.3	.74	.061
1.00	0.0	4.0	-1.5	1.06	.108	.096	158.0	.71	.056
1.17	0.0	2.2	-1.6	1.05	.100	.074	155.5	.69	.044
1.33	0.0	.64	-1.5	1.03	.070	.019	152.6	1.14	.029
1.50	0.0	.20	-1.5	1.02	.039	.0020	151.0	1.20	.015
1.67	0.0	.10	-1.4	1.02	.017	.000070	150.7	1.24	.008
0.0	.33	4.0	7.5	1.09	.126	.14	163.0	.64	.063
0.0	.50	3.0	6.5	1.12	.123	.14	166.9	1.04	.060
0.0	.67	2.5	4.7	1.12	.127	.17	166.2	1.08	.060
0.0	.83	2.2	3.4	1.11	.127	.17	157.8	1.03	.061

TABLE B-4 (Continued)

X/R	Y/R	Flow Pitch (DEG)	Flow Yaw (DEG)	U_z/U_E	$*\sqrt{\overline{v'^2}}/U_E$	$(x10^2)$ $*\overline{u'v'}/U_E^2$	V_{Total} (fps)	$P_{st}-P_{st\infty}$ (psf)	$\sqrt{\overline{u'^2}}/U_E$
0.0	1.0	1.7	2.0	1.08	.118	.14	153.9	1.12	.059
0.0	0.0	4.1	-1.6	1.02	.127	.168	146.3	-.92	.069
0.0	-.17	3.4	-8.7	1.05	.119	.167	152.1	-.95	.068
0.0	-.33	2.3	-13.9	1.09	.111	.125	160.3	-.76	.063
0.0	-.50	1.4	-12.7	1.11	.108	.089	162.2	-.09	.060
0.0	-.67	.84	-9.2	1.11	.108	.079	160.9	.29	.060
0.0	-.83	.64	-7.5	1.10	.107	.071	158.3	.60	.062
0.0	-1.0	.49	-6.1	1.07	.100	.056	154.2	.80	.059
0.0	-1.17	.34	-4.7	1.06	.087	.033	151.5	1.01	.053
0.0	-1.33	.30	-3.3	1.05	.070	.014	149.9	1.14	.042
0.0	-1.50	.25	-2.2	1.04	.049	.0034	148.5	1.26	.030
0.0	-1.67	.25	-1.6	1.03	.032	.00057	146.9	1.38	.017
0.0	-1.83	.30	-1.2	1.02	.019	.00007	146.0	1.39	.008
0.0	-2.0	.25	-1.2	1.02	.0096	.000008	146.0	1.42	.006
0.0	1.17	1.3	1.0	1.04	.100	.074	149.1	.39	.053
0.0	1.33	.94	-.16	1.01	.076	.022	144.7	.42	.038
0.0	1.50	.64	-1.1	.99	.051	.0047	142.3	1.01	.028
0.0	1.67	.64	-1.5	.98	.038	.0015	141.1	.99	.021
0.0	1.83	.59	-1.6	.99	.032	.00091	142.7	1.49	.019
0.0	2.00	.59	-1.7	.98	.032	.00090	142.3	1.46	.019
0.0	2.17	.54	-1.7	.98			142.3	1.46	.019
0.0	2.33	.49	-1.7	.98			142.3	1.46	.019
-1.67	2.00	0.0	-1.6	1.02	S	S	148.4	1.67	.005
-1.33	2.00	0.0	-1.6	1.02	S	S	148.3	1.62	.006
-1.17	2.00	0.0	-1.6	1.02	S	S	148.0	1.58	.008
-1.00	2.00	.10	-1.6	1.02	S	S	148.1	1.60	.012
-.83	2.00	.25	-1.5	1.01	S	S	147.6	1.59	.016

TABLE B-4 (Continued)

X/R	Y/R	Flow Pitch (DEG)	Flow Yaw (DEG)	U_z/U_E	$*\sqrt{\overline{v'^2}}/U_E$	$(x10^2)$ $*\overline{u'v'}/U_E^2$	V_{Total} (fps)	$P_{st}-P_{st\infty}$ (psf)	$\sqrt{\overline{u'^2}}/U_E$
-.67	2.00	.34	-1.5	1.01	S	S	146.5	1.52	.019
-.50	2.00	.34	-1.6	1.00	S	S	145.2	1.50	.021
-.33	2.00	.44	-1.6	.99	S	S	143.8	1.47	.020
-.17	2.00	.59	-1.7	.99	S	S	143.7	1.48	.020
0.0	2.00	.64	-1.7	.98	.037	.00059	142.7	1.40	.019
.17	2.00	.59	-1.7	.98	.038	.00063	143.0	1.41	.020
.33	2.00	.49	-1.8	.99			143.8	1.40	.021
.50	2.00	.44	-1.9	.99	.034	.0037	144.7	1.38	.021
.67	2.00	.39	-1.9	1.00	.028	.0043	146.1	1.40	.019
.83	2.00	.30	-2.0	1.01	.022	.00068	147.2	1.35	.015
1.0	2.00	.25	-2.0	1.02	.016	.00018	148.3	1.38	.010
1.17	2.00	.25	-2.0	1.02	.012	.000062	148.6	1.37	.007
1.33	2.00	.30	-1.9	1.02	.0097	.000031	148.7	1.31	.005

* Measurements taken in high flow angularity

S Symmetric profiles

TABLE B-5

Profiles for Z/D = 40, α_e = 0°

X/R	Y/R	Flow Pitch (DEG)	Flow Yaw (DEG)	U_z/U_E	$*\sqrt{\overline{v'^2}}/U_E$	$(x10^2)$ $*\overline{u'v'}/U_E^2$	V_{Total} (fps)	$P_{st}-P_{st\infty}$ (psf)	$\sqrt{\overline{u'^2}}/U_E$
.33	0.0	.64	-.25	1.04	.0446	.00132		1.44	
.67	0.0	.69	0.0	1.03	.0358	.000725		1.42	.0232
1.00	0.0	.54	-.65	1.02	.0351	.000674		1.27	.0217
1.33	0.0	.54	-.25	1.01	.0351	.000621		1.22	.0200
1.67	0.0	.49	-.15	1.01	.0324	.000407		1.19	.0167
2.00	0.0	.39	-.10	1.00	.0311	.000315		1.09	.0143
2.33	0.0	.34	.05	1.00	.0243	.000134		1.09	.0113
2.67	0.0	.25	0.0	1.00	.0182	.000041		1.07	.0075
0.0	0.0			1.08	.0514	.00199			.0268
0.0	-.17			1.08	.0487	.0015			.0267
0.0	-.33			1.07	.0453	.0011			.0250
0.0	-.83			1.06	.0420	.00074			.0232
0.0	-1.00			1.06	.0399	.00056			.0225
0.0	-1.17			1.05					.0217
0.0	-1.33			1.05	.0351	.000361			.0208
0.0	-1.50			1.05					.0200
0.0	-1.67			1.04	.0311	.000240			.0175
0.0	-1.83			1.04					.0158
0.0	-2.00			1.04	.0257	.000109			.0153
0.0	-2.17			1.04					.0134
0.0	-2.33			1.03	.0203	.000038			.0117
0.0	-2.50			1.03					.0095
0.0	-2.83			1.03	.0108	.0000055			.0073
0.0	-3.17			1.03					.0063
0.0	.17			1.05	.0534	.00242			.0275

TABLE B-5 (Continued)

X/R	Y/R	Flow Pitch (DEG)	Flow Yaw (DEG)	U_z/U_E	$*\sqrt{\overline{v'^2}}/U_E$	$(x10^2)$ $*\overline{u'v'}/U_E^2$	V_{Total} (fps)	$P_{st}-P_{st\infty}$ (psf)	$\sqrt{\overline{u'^2}}/U_E$
0.0	.33			1.05	.0527	.00240			.0267
0.0	.50			1.05					.0258
0.0	.67			1.04	.0473	.00167			.0242
0.0	.83			1.04					.0233
0.0	1.00			1.04	.0453	.00129			.0225
0.0	1.17			1.03					.0225
0.0	1.33			1.03	.0446	.00127			.0225
0.0	1.50			1.02					.0225
0.0	1.67			1.02	.0432	.00121			.0225
0.0	1.83			1.01					.0208
0.0	2.00			1.00	.0378	.00079			.0183
0.0	2.17			1.00					.0167
0.0	2.33			1.00	.0324	.00041			.0157
.17	0.0			1.04					.0258
0.0	2.33			1.00	.0324	.00041			.0157
.17	2.33			1.00	.0324	.00038			.0158
.33	2.33			1.00	.0324	.00037			.0153
.50	2.33			1.00					.0153
.67	2.33			1.00	.0324	.00030			.0150
.83	2.33			1.00					.0143
1.00	2.33			1.00	.0284	.000185			.0135
1.17	2.33			1.01					.0125
1.33	2.33			1.01	.0243	.000087			.0112
1.50	2.33			1.01					.0098
1.67	2.33			1.01	.0189	.000036			.0087
1.83	2.33			1.01					.0077

TABLE B-5 (Continued)

X/R	Y/R	Flow Pitch (DEG)	Flow Yaw (DEG)	U_z/U_E	$*\sqrt{\overline{v'^2}}/U_E$	$(x10^2)$ $*\overline{u'v'}/U_E^2$	V_{Total} (fps)	$P_{st}-P_{st\infty}$ (psf)	$\sqrt{\overline{u'^2}}/U_E$
2.00	2.33			1.01	.0142	.000014			.0065
2.17	2.33			1.01					.0060
2.50	2.33			1.01	.0108	.000007			.0057

* Measurements taken in high flow angularity

TABLE B-6

Profiles for Z/D = 40, α_e = -2°

X/R	Y/R	Flow Pitch (DEG)	Flow Yaw (DEG)	U_z/U_E	$*\sqrt{\overline{v'^2}}/U_E$	$(x10^2)$ $*\overline{u'v'}/U_E^2$	V_{Total} (fps)	$P_{st}-P_{st\infty}$ (psf)	$\sqrt{\overline{u'^2}}/U_E$
3.0	0.0			.99	.0182	.000023			.0063
2.67	0.0			.99	.0203	.000043			.0090
2.33	0.0			.99	.0264	.000123			.0093
2.00	0.0			.99	.0304	.00032			.0130
1.67	0.0			.99	.0351	.00051			.0165
1.33	0.0			1.00	.0365	.00058			.0183
1.00	0.0			1.00	.0365	.00059			.0200
.67	0.0			1.00	.0351	.00046			.0200
.33	0.0			1.00	.0331	.00036			.0200
0.0	0.0			1.00	.0365	.00046			.0200
0.0	-.17			1.06	.0405	.00055			.0192
0.0	-.33			1.05	.0392	.00048			.0192
0.0	-.67			1.03	.0345	.00031			.0183
0.0	-1.00			1.02	.0297	.00019			.0167
0.0	-1.33			1.02	.0270	.00013			.0143
0.0	-1.67			1.01	.0243	.000083			.0122
0.0	-2.33			1.00	.0189	.000028			.0063
0.0	-2.67			1.00	.0185	.000023			.0057
0.0	-3.00				.0182	.000023			
0.0	.33			1.02	.0446	.00094			.0225
0.0	.67			1.02	.0514	.00164			.0250
0.0	1.0			1.02	.0554	.00263			.0258
0.0	1.33			1.02	.0427	.00207			.0233
0.0	1.67			1.01	.0500	.00157			.0225
0.0	2.00			1.00	.0487	.00153			.0232

TABLE B-6 (Continued)

X/R	Y/R	Flow Pitch (DEG)	Flow Yaw (DEG)	U_z/U_E	$*\sqrt{\overline{v'^2}}/U_E$	$(x10^2)$ $*\overline{u'v'}/U_E^2$	V_{Total} (fps)	$P_{st}-P_{st\infty}$ (psf)	$\sqrt{\overline{u'^2}}/U_E$
.33	2.33			.98	.0500	.00150			.0160
.67	2.33			.98	.0500	.00141			.0140
1.00	2.33			.98	.0487	.00111			.0117
1.33	2.33			.99	.0432	.00072			.0088
1.67	2.33			.99	.0365	.00038			.0075
2.00	2.33			.99	.0284	.00015			.0063
2.33	2.33			.99	.0230	.000060			.0057
2.67	2.33				.0209	.000041			
3.00	2.33				.0203	.000035			

*Measurements taken in high flow angularity

S Symmetric profiles

The vita has been removed from the scanned document

MEAN FLOW AND TURBULENCE MEASUREMENTS IN THE WAKE OF A SLENDER PROPELLER-DRIVEN BODY INCLUDING EFFECTS OF PITCH ANGLE

by

Edward Bruce Daffan

ABSTRACT

An experimental study of the turbulent wake produced by a stern-propeller-driven body at pitch angles of 0^{o} and -2^{o} is presented. The effect of an appendage such as a submarine sail to an axisymmetric body is also considered. Mean flow velocities, static pressure, flow angularity, and turbulence quantities are presented at three downstream stations Z/D = 2, 10, and 40. The measurements were taken using a yawhead pressure probe and hot-wire sensors. The testing was conducted in the Virginia Tech 6-foot subsonic tunnel at free-stream $Re_D \simeq 4.4 \times 10^5$. The addition of the appendage substantially increased the drag on the slender axisymmetric body considered and increased the turbulence level in the region behind the sail. The propeller swirl was also decreased by the presence of the sail. The results for the negative pitch angle indicate further increases in the turbulence intensities and a greater decrease in the swirl behind the sail.